Hybrid Path Integral Monte Carlo/Molecular Dynamics Approach for the Simulation of Rigid Rotating and Translating Molecules

by

Xichen Lou

A thesis

presented to the University of Waterloo

in fulfillment of the

thesis requirement for the degree of

Master of Science in

Chemistry

Waterloo, Ontario, Canada, 2019

Author's Declaration

I hereby declare that I am the sole author of this thesis. This is a true copy of the thesis, including any required final revisions, as accepted by my examiners.

I understand that my thesis may be made electronically available to the public.

Abstract

The path integral formulation of quantum statistical mechanics [1] is a widely used approach to express the partition function and obtain estimators for diverse thermodynamic properties of molecular systems. The main objective of this thesis is to propose new approaches to simulate the translations and rotations of rigid molecular systems and test these methodologies via benchmark calculations.

We first present benchmark calculations based on a newly developed Path Integral Monte Carlo (PIMC) code for rigid body rotations implemented in the Molecular Modelling Toolkit software package [2]. Our rigid body PIMC simulation results are compared with the exact diagonalization calculation for the rigid Hydrogen Fluoride trapped in an electric field. An energy convergence study allows us to establish the validity of the new PIMC code within statistical error. We then benchmark our PIMC code against the direct Classical Monte Carlo (dCMC) calculations to study the interacting quantum rotors at finite temperature. The quantum and classical calculations are expected to agree at high temperature when classical statistical mechanics is valid. The dCMC code is then used to study a 1D water chain system at different temperatures and lattice spacings. Two phase transitions and three specific phase regions have been observed from the calculations.

We then combine a well-established translational Path Integral Molecular Dynamics

(PIMD) code [3, 4] with the rigid body PIMC code to develop a novel hybrid PIMD/PIMC program to simulate the quantum molecular dynamics of molecular systems with both rotational and translational degrees of freedom. This proposed methodology is successfully benchmarked for the CO_2-He system for a range of imaginary time steps.

The second PIMC methodology introduces a cluster-update algorithm to sample rigid body Feynman paths associated with quantum rotations. This cluster-update methodology has been previously applied to lattice spin systems [5, 6] and hard spheres in the continuum [7]. To our knowledge, this is the first time one develops a cluster-update method for quantum rotors with anisotropic interactions. An initial cluster-update PIMC algorithm and its associated test calculations are presented. Preliminary results for Hydrogen Fluoride molecules with dipole-dipole interactions reveal issues with our initial algorithm. The source of the problem is fully discussed in this thesis and will law the foundation for further studies.

Overall, this thesis focuses on the development of new methodologies to study quantum motions of molecules at finite temperature. We note that additional tests and benchmark calculations will be required to further validate the methodologies and algorithms we have developed. This thesis nevertheless presents and discusses novel methodological advancements and applications and will lead to exciting new directions.

Acknowledgements

I would like to thank my undergraduate and graduate supervisor, Prof. Pierre-Nicholas Roy. His endless ideas and encouragement make me possible to achieve more than I thought. His patience and enthusiasm for research and life influence me and lead a positive atmosphere in the group. Even he is occupied with meetings or conferences outside of campus, he is willing to help anyone in the group for which I am pretty grateful. He helped me with not only academic problems but also my study permit as an international student.

I also would like to acknowledge several past graduate students, especially Matthew Schmidt, he helped me when I was an undergraduate student. He was patient with my basic questions and helped me with programming on what I use in this thesis.

Also, the best Theoretical Chemistry group, I would like to thank Tapas Sahoo, our Post-doc, he helped me with benchmarking calculations, and he is very nice and patient on every question I asked. His professional suggestions support me to finish my coding and calculations. And PhD student, Dmitri Iouchtchenko provided creative ideas and helped me with any technical problems I had, and Kevin Bishop helped me with the water force field model setup in our code.

I would also like to thank the rest of my Advisory Committee members, including

Professor Marcel Nooijen and Professor Jeff Chen.

Finally, I acknowledge the rest of the Roy group, namely Xiaolong Zhang, Spencer Yim, Neil George Raymond, Jianying Sheng, Alexander Ibrahim, and Adam Robert Marr for the great research atmosphere.

Dedication

This thesis is to my friends who helped me when I was in trouble, and my beloved family, especially to my mother: Liqiong Yao.

Table of Contents

List of Tables

List of Figures

Abbreviations

dCMC direct Classical Monte Carlo Method 20

GCA Geometric Cluster Algorithm 30

H_2O@SWCNT Water in Single Wall Carbon Nanotube 13

MB-Pol Many Body - Polarizable 36

MLR Morse/long-range potential 15

MMTK Molecular Modelling Toolkit 2, 15

MoRiBS Molecular rotors in bosonic solvents simulation program 16

PI Path Integral 1, 5

PILE Path Integral Langevin Equation 2, 15, 19

PIMC Path Integral Monte Carlo 2, 15, 19

PIMD Path Integral Molecular Dynamics 2, 15

q-SPC/FW Quantum Simple Point Charge Flexible Water 36

q-TIP4P/F Quantum Transferable Intermolecular Potential with 4 Points Flexible 36

SWCNT Single Wall Carbon Nanotube 13

Chapter 1

Introduction

Computational chemistry uses the fundamental principles of chemistry and physics along with mathematical modelling and computational algorithms in order to develop computer programs to simulate and predict the properties of molecular systems. Although many properties can be measured in the laboratory, some measurements are currently out of the reach of current experimental setups. The quantum many-body problem, in particular, is always a topic of central importance for both experimental and theoretical chemistry. In order to describe the quantum many-body system and understand the details of the microstates, a computational simulation is a good approach to tackle this problem.

The various modes of motion of molecular systems, such as translations, vibrations, and rotations, are quantum mechanical in nature and their inclusion in a computer simulation is a formidable task when many molecules are present. In 1948, Feynman developed the so-called Path Integral (PI) formulation [10] which allows scientists to compute and predict the thermodynamic properties of these quantum systems. From then on, scientists have been able to combine the path integral formulation with different computational methods

to simulate various many-body quantum systems at finite temperature. One of the most well-established methods is Path Integral Monte Carlo (PIMC) based on Metropolis sampling [66] which allows one to calculate the temperature-dependent properties of quantum systems [11, 12, 13]. Also, another approach, Path Integral Molecular Dynamics (PIMD), has been developed recently to describe these systems without pure random walks but molecular dynamics samplings to simulate quantum motions [14, 15]. Those approaches and algorithms are implemented in the scientific computer package Molecular Modelling Toolkit (MMTK) [2], an open-source Python-based platform for the development of molecular simulation software.

In this thesis, the rotational contribution to the properties of a quantum system is computed with PIMC in MMTK and the treatment of the translational degree of freedom is based on PIMD with Path Integral Langevin Equation (PILE) thermostat [16] for finite temperature systems. Then, the validity of the hybrid PIMD/PIMC approach is discussed. Furthermore, a new cluster-update Monte Carlo algorithm is introduced to solve the non-ergodic problem PIMC simulation based on earlier studies [5, 6, 7].

1.1 Theory

1.1.1 Statistical Mechanics and Path Integral Formulation

Statistical mechanics is considered the most powerful tool for scientists to apply statistics theory on the microscopic properties of atoms or molecules to understand the thermodynamic properties of macrosopic systems. According to quantum statistical mechanics, an ensemble, which is a collection of microstates, can reach thermodynamic equilibrium over a long time or simulation. The fundamental postulate of equilibrium statistical mechanics defines equal a priori probabilities. The statement can be summarized as: all accessible microstates have the equal probability for an equilibrium isolated system. Thus, the canonical partition function can be evaluated by the Boltzmann factor with the equal a priori probabilities postulate which stores all thermodynamic information. It is a sum or a trace in matrix expression of all microstates. In general equilibrium canonical ensemble, the number of particles (N), the volume (V), and also the temperature (T) are fixed for systems. The Hamiltonian of an N-particle system consists of translational and rotational motions with particle interaction is given by,

$$\hat{H} = \hat{T}_{\text{trans}} + \hat{T}_{\text{rot}} + \hat{V} \tag{1.1}$$

also, the rigid molecules approximation is assumed, which neglects the centrifugal distortion and rotational-vibrational coupling. For simplicity, the expressions below only describe one-particle system. Thus, the partition function is given by

$$Z(\beta) = \mathrm{Tr}(e^{-\beta\hat{H}}) \tag{1.2}$$

$$= \mathrm{Tr}(\hat{\rho}(\beta)) \tag{1.3}$$

in this thesis, $\hat{\rho}(\beta) = e^{-\beta\hat{H}}$ shall always mean the thermal density matrix or imaginary time "propagator", and it will not be normalized by the partition function. β here is always real and defined as follows, which is also called the imaginary projection time,

$$\beta = \frac{1}{k_B T} \tag{1.4}$$

where k_B is the Boltzmann constant, and T is the temperature of the system.

Hence, the expectation value of an observable $\hat{\mathcal{O}}$ can be calculated by partition function as follows

$$\langle\hat{\mathcal{O}}\rangle = \frac{1}{Z(\beta)}\mathrm{Tr}\{\hat{\mathcal{O}}\hat{\rho}(\beta)\} \tag{1.5}$$

Use the properties of exponential, we have

$$\hat{\rho}(\beta) = (e^{-\beta \hat{H}/P})^P \tag{1.6}$$

$$= [\hat{\rho}(\beta/P)]^P \tag{1.7}$$

Now, the exponential part is separated into P discrete slices which is defined as the Trotter slices [17] or the quantum beads. We can define $\tau = \beta/P$, which is named as the imaginary time step. Also, $\hat{\rho}(\beta/P) = \hat{\rho}(\tau)$, and τ corresponds to a higher temperature.

In quantum mechanics, we know the kinetic operator and the potential operator do not commute, so the expression below is not equal for both sides.

$$\hat{\rho}(\beta) = e^{-\beta(\hat{T}_{\text{trans}} + \hat{T}_{\text{rot}} + \hat{V})} \neq e^{-\beta(\hat{T}_{\text{trans}} + \hat{T}_{\text{rot}})} e^{-\beta \hat{V}} \tag{1.8}$$

Then, we can apply the Trotter factorization formula [17] to the high temperature density matrix $\hat{\rho}(\tau)$. We also have the expression as below which is the basis for the Feynman PI formulation [10], the error order of this expression is a quadratic magnitude of τ [18].

$$\hat{\rho}(\tau) = e^{-\tau(\hat{V}+\hat{T}_{\text{trans}}+\hat{T}_{\text{rot}})} \tag{1.9}$$

$$\approx e^{-\tau\hat{V}} e^{\tau(\hat{T}_{\text{trans}}+\hat{T}_{\text{rot}})} \tag{1.10}$$

Then, in symmetric form we have [17, 19]

$$\hat{\rho}(\tau) \approx e^{-\tau\hat{V}/2} e^{-\tau(\hat{T}_{\text{trans}}+\hat{T}_{\text{rot}})} e^{-\tau\hat{V}/2} \tag{1.11}$$

$$\hat{\rho}(\beta) = \lim_{P\to\infty} \left\{ e^{-\tau\hat{V}/2} e^{-\tau(\hat{T}_{\text{trans}}+\hat{T}_{\text{rot}})} e^{-\tau\hat{V}/2} \right\}^P \tag{1.12}$$

As for both the translation and rotation are considered in our system, the position and the orientation of the molecule of each bead are defined as $\{\mathbf{q_t}, \omega_t\}$. Here, $\mathbf{q_t}$ stands for the position of the molecule's the center of mass translations, and ω_t denotes the orientation of the molecule in rotations. Due to the rigid body approximation, $\hat{T}_{\text{trans}}$ and $\hat{T}_{\text{trans}}$ do commute, we can insert the identities $\mathbb{1}_t$ at each Trotter slices $t = 1, 2, 3 \cdots, P$

$$\mathbb{1}_t = \int d\mathbf{q}_t \int d\omega_t |\mathbf{q}_t\omega_t\rangle\langle\mathbf{q}_t\omega_t| \tag{1.13}$$

in the partition function expression and a cyclic form can be generated as which is the path integral formulation:

$$\begin{aligned} Z = \lim_{P\to\infty} (& \int d\mathbf{q}_1 \int \omega_1 \int d\mathbf{q}_2 \int \omega_2 \cdots \int d\mathbf{q}_{P-1} \int \omega_{P-1} \int d\mathbf{q}_P \int d\omega_P \\ & \rho_{1,P}(\tau) \times \rho_{P,P-1}(\tau) \times \cdots \times \rho_{3,2}(\tau) \times \rho_{2,1}(\tau)) \end{aligned} \tag{1.14}$$

where $\rho_{t,t+1}(\tau) \equiv \rho_{t,t+1}(\tau; \mathbf{q}_t, \mathbf{q}_{t+1}, \omega_t, \omega_{t+1})$ is the shortcut for the general high-temperature density matrix element in the $\{\mathbf{q_t}, \omega_t\}$ representation. Since $\hat{V}$ is diagonal in coordinate space and can be expressed as $V(\mathbf{q}, \omega)$. Then, the density matrix elements, $\rho_{t,t+1}(\tau)$, for different components can be expressed as follows,

$$\rho^{\text{pot}}_{t,t+1}(\tau; \mathbf{q}_t, \mathbf{q}_{t+1}, \omega_t, \omega_{t+1}) = e^{(-\frac{\tau}{2}\{V(\mathbf{q}_t,\omega_t)+V(\mathbf{q}_{t+1},\omega_{t+1})\})} \tag{1.15}$$

$$\rho^{\text{trans}}_{t,t+1}(\tau; \mathbf{q}_t, \mathbf{q}_{t+1}) = \langle\mathbf{q}_t|e^{-\tau\hat{T}^{\text{trans}}}|\mathbf{q}_{t+1}\rangle \tag{1.16}$$

$$\rho^{\text{rot}}_{t,t+1}(\tau; \omega_t, \omega_{t+1}) = \langle\omega_t|e^{-\tau\hat{T}^{\text{rot}}}|\omega_{t+1}\rangle \tag{1.17}$$

In terms of computational consideration, the Trotter limit $P \to \infty$ cannot be achieved in practice, so a sufficiently large P can be chosen in computing to achieve a result within acceptable statistical erros.

Then, we insert another identity in terms of momentum basis $\mathbf{p}$, $\mathbf{1} = \int d\mathbf{p}_t |\mathbf{p}_t\rangle\langle\mathbf{p}_t|$, to evaluate the translational contribution of density matrix element

$$\rho^{\text{trans}}_{t,t+1}(\tau; \mathbf{q}_t, \mathbf{q}_{t+1}) = \int d\mathbf{p}_t \langle \mathbf{q}_t | e^{-\tau \hat{T}^{\text{trans}}} | \mathbf{p}_t \rangle \langle \mathbf{p}_t | \mathbf{q}_{t+1} \rangle \tag{1.18}$$

Thus, the translational contribution of the density matrix can be analytically calculated,

$$\rho^{\text{trans}}_{t,t+1}(\tau; \mathbf{q}_t, \mathbf{q}_{t+1}) = \left(\frac{mP}{2\pi\hbar^2\beta} \right)^{d/2} \exp\left[-\frac{mP}{2\hbar^2\beta} (\mathbf{q}_t - \mathbf{q}_{t+1})^2 \right] \tag{1.19}$$

where d is the dimension of space for translational system, for 3D system $d = 3$.

As for the rotational contribution of the density matrix elements, we can still insert an identity operator composed of free-rotor wave functions. However, the rotational motion is far more complicated than translation, and the expressions also depend on the symmetry of different molecules.

1.1.2 Path Integral Formulation for Linear Rotor

After evaluating the analytical density matrix element of translational and potential contributions, we now try to evaluate the rotational component. However, the rotational part $\rho^{\text{rot}}_{t,t+1}$ is different due to the distinct dimension of rotors. The most important rotor model is the rigid rotor approximation of the linear rotor and asymmetric top rotor, in this section, the path integral formulation for linear rotors is presented.

In terms of linear rotor, the orientation of a particle can be determined by two angles $\Omega = (\theta, \varphi)$, the rotational operator can be expressed as [11]

$$\hat{T}^{\text{linrot}} = -B\left(\frac{\partial^2}{\partial\theta^2} + \cot\theta\frac{\partial}{\partial\theta} + \frac{1}{\sin^2\theta}\frac{\partial^2}{\partial\varphi^2}\right) \tag{1.20}$$

where B is the rotational constant for linear molecules, after a similar process of inserting an identity operator in momentum representation, it gives the density matrix elements expression as [20]

$$\rho^{\text{linrot}}_{t,t+1}(\tau;\omega_t,\omega_{t+1}) = \sum_{J=0}^{\infty}\frac{2J+1}{4\pi}P_J(\mathbf{e}_t\cdot\mathbf{e}_{t+1})e^{-\frac{\beta}{P}J(J+1)B} \tag{1.21}$$

where J is the rotational quantum number, $\mathbf{e}_t$ indicates the normalized orientation vector of the molecule at Trotter slice t, and P_J is the Legendre polynomial of J.

By applying the thermodynamic relation of internal energy and partition functioin $U(\beta) = -\partial \ln Z(\beta)/\partial\beta$, the primitive rotational energy estimator can be obtained [13]

$$\begin{aligned} T^{\text{linrot}} &= \frac{1}{P}\sum_{t=1}^{P} T_t^{est} \\ T_t^{\text{linrot}} &= \frac{B}{4\pi\rho_{t,t+1}^{linrot}}\sum_{J}(2J+1)J(J+1)P_J(\mathbf{e}_t\cdot\mathbf{e}_{t+1})e^{-\frac{\beta}{P}J(J+1)B} \end{aligned} \tag{1.22}$$

1.1.3 Path Integral Formulation for Non-linear Rotors

As for the asymmetric top rotor, the orientation is normally defined by three Euler angles $\omega = (\varphi, \theta, \chi)$. Also, the rotational transformation can be expressed by the related rotational matrix $\vec{R}$ which will transform the space coordinates into the body frame.

In addition to the representation of the orientation, the rotational constants of a non-linear rotor are also different from the linear ones'. There are three principal moments of inertia $(\Theta_{aa}, \Theta_{bb}, \Theta_{cc})$ determined three rotational constants (A, B, C). And the non-linear rotors can be categorized by the values of three moments of inertia, a molecule is called asymmetric top if $\Theta_{aa} < \Theta_{bb} < \Theta_{cc}$, spherical top if $\Theta_{aa} = \Theta_{bb} = \Theta_{cc}$, oblate symmetric top if $\Theta_{aa} = \Theta_{bb} < \Theta_{cc}$, prolate symmetric top if $\Theta_{aa} < \Theta_{bb} = \Theta_{cc}$. In our project, we now only consider about the most complicated case: the asymmetric top.

As we know, the basis set eigenfunction of the symmetric top is defined as $|JMK\rangle$,

where J is the total angular momentum, M is the space-fixed projection angular momentum, K is the body-fixed projection angular momentum. Also, the eigenfunctions of the asymmetric top can be expanded in the basis set eigenfunctions of symmetric top $|JMK\rangle$, which gives

$$|JM\tilde{K}\rangle = \sum_{K} A_{\tilde{K}K}^{(JM)} |JMK\rangle \tag{1.23}$$

where $A_{\tilde{K}K}^{(JM)}$ is the eigenvector from the diagonalization of the symmetric top basis set and can be considering as the linear combination coefficient.

The density matrix elements for an asymmetric top can now be evaluated by inserting the identity operator based on the basis set of eigenfunction $|JM\tilde{K}\rangle$ similarly, then it gives [21]

$$\begin{aligned}\rho_{t,t+1}^{\text{asymrot}}(\tau;\omega_t,\omega_{t+1}) = \sum_{J=0}^{\infty} \frac{2J+1}{8\pi^2} \sum_{M=-J}^{J} \sum_{\tilde{K}=-J}^{J} d_{MM}^{J}(\tilde{\theta}_{t,t+1}) \cos[M(\tilde{\varphi}_{t,t+1} + \tilde{\chi}_{t,t+1})] \\ \times \left| A_{\tilde{K}M}^{(JM)} \right|^2 \exp\left[-\tau E_{\tilde{K}}^{(JM)} \right]\end{aligned} \tag{1.24}$$

where $d_{MK}^{J}(\theta)$ represents Wigner reduced d-matrix [22], $\tilde{\Omega} = (\tilde{\theta}, \tilde{\varphi}, \tilde{\chi})$ are the Euler

angles (related definition for Euler angles can be found in Appendix A.2) which are defined in a laboratory frame where the Euler angles of t slice are set to zero ($\Omega_t = (0, 0, 0)$), $E_{\tilde{K}}^{(JM)}$ is the eigenenergy.

While obtaining the density matrix, it is also available to evaluate the rotational energy estimator [21],

$$\begin{aligned} T_{t,t+1}^{\text{asymrot}} =& \frac{1}{\rho_{t,t+1}^{asymrot}} \sum_{JM\tilde{K}} \left(\frac{2J+1}{8\pi^2} \right) A_{\tilde{K}M}^{(JM)} E_{\tilde{K}}^{(JM)} \\ & \times \exp\left(-\tau E_{\tilde{K}}^{(JM)} \right) \sum_{K} A_{\tilde{K}K}^{(JM)} d_{MK}^{J}(\tilde{\theta}_{t+1}) \\ & \times \cos(M\tilde{\varphi}_{t+1} + K\tilde{\chi}_{t+1}) \end{aligned} \tag{1.25}$$

1.2 Confined Quantum Molecules

We're interested in confined molecules, not only molecules trapped in the hard cages such as fullerenes but also the soft cages like solvent superfluid helium. The spectra of molecules confined in these environments retained features associated with gas-phase behaviour.

1.2.1 Endofullerene

Molecular endofullerenes have been synthesized and studied in previous experiments [23, 24]. The encapsulated small molecules are able to freely rotate and translate inside the fullerene. Dipolar molecules such as hydrogen fluoride in C_{60} ($HF@C_{60}$) and water in C_{60} ($H_2O@C_{60}$) are isolated by the bulky cage which has no hydrogen bonding or other complex interactions. The quantized translational and rotational motions have been discovered by spectrum experiments [23], also the potential surface of molecules trapped in fullerenes is well-studied [25, 26]. Since the previous theoretical simulations [27, 28, 29] for the endofullerene system focused on the free translation behaviour, the rotational and related dipolar behaviour aroused great interest.

1.2.2 Water confined in Single Wall Carbon Nanotubes

Molecules can be confined not only into the above fullerene cages but also in other forms of carbon such as single-wall carbon nanotubes. Single Wall Carbon Nanotube (SWCNT) is one of the most well-studied systems to study nano-confined molecules, especially Water in Single Wall Carbon Nanotube ($H_2O@SWCNT$). Since water is the most important component of transportation fluids in biology, the SWCNT provides a very interesting analogue model of natural systems to study the behaviour of nanoconfined water [30, 31].

Confined water molecules exhibit unusual behaviours such as sensitive ion selectivity [32] and anomalously low friction and superior flow [33, 34]. Recent studies have also revealed that confined water molecules in carbon nanotubes have excellent water permeability which may suggest novel water purification systems [35, 36].

Recent experiments on quasi-1d water chains in SWCNT have revealed an anomalous hydrogen bond network and also a temperature-dependent quasi-phase transition [37, 38, 39]. In this thesis, we will implement both classical and quantum simulations for such a system in order to explore the behaviour of a simplified 1D water chain inspired by these experiments.

1.2.3 Molecules doped in superfluid clusters

Unlike the hard cage introduced above, the superfluid solvent is a kind of "soft" confinement for molecules. The lack of viscosity makes it possible for quantum mechanics to be manifested in a liquid system instead of a discrete atom system. ^{4}He is the first and macroscopic superfluid observed in 1938 at a low temperature [40]. The experiments were done by previous studies [41] for rotors in superfluid ^{4}He indicates a high-resolved rotational spectrum and sharp rotational transitions. In terms of theoretical simulations of the microscopic superfluid system, an accurate potential energy surfaces (PES) is required to describe the interactions. A well known analytical function for CO_2-He system is developed

and proved by Le Roy et al: Morse/long-range potential (MLR) [42]. The MLR formula for the He-He interactions is also introduced by Christopher Ing et al based on Aziz He-He potential [3]. With the accurate and efficient potential model, it is able to simulate the system of CO_2 doped Helium cluster with PIMD or PIMC methods [3]. Li et al's group and Zeng et al's group studied for the cluster doped linear and non-linear rotors respectively with PIMC simulation. In 2012, Ing et al performed the PIMD simulation with PILE with doped helium clusters. More research on the simulations of the microscopic superfluidity can be found in this field with both PIMD and PIMC method [43, 44]. In this thesis, we will prove the validity of a hybrid PIMC/PIMD approach for the simulation of such soft cages systems by benchmarking against the previous well-studied simulation program.

1.3 Outline of the thesis

This thesis focuses on the development of methods based on the path integral formulation of quantum statistical mechanics to simulate molecular systems and determine their energetic and structural properties. In Chapter 2, we introduce and compare the different Monte Carlo methods and PIMD. Following this discussion, benchmark calculations are performed in Chapter 3 to establish the validity and accuracy of the newly implemented PIMC code in MMTK. In Chapter 4, we apply our method to simulate a 1D water chain with only

rotational motion for a wide range of temperatures and lattice spacings and compare the energy and orientational behaviour with the direct Classical Monte Carlo method to explore a possible phase transition. In Chapter 5, a hybrid PIMD/PIMC method is implemented and introduced to simulate the translational and rotational motion of quantum systems. We test the validity of this method for a CO_2 doped Helium system and compare our results with the PIMC method implemented in the Molecular rotors in bosonic solvents simulation program (MoRiBS) [45]. Chapter 6 discusses and develops a new methodology for cluster Monte Carlo with rotors. Finally, Chapter 7 summarizes the most important findings and conclusions of this thesis. Future developments and associated applications are also proposed in this last chapter.

Chapter 2

Computational Methodologies

The main contribution of this thesis is to confirm the validity of our hybrid PIMD/PIMC program to simulate translating and rotating molecules under quantum mechanical conditions. Thus, it is necessary to comprehend the fundamental knowledge of those methods, and also their related advantages and disadvantages. Moreover, the reason why we chose those methods to simulate our system is also important in our topic. This chapter will show the reasons and give a basic introduction to our computational methodologies.

2.1 Path Integral Molecular Dynamics

One of the main methods to simulate finite temperature translating molecules is using path integral formulation with molecular dynamics method [46]. PIMD treats the quantum system as a classical ring polymer system with P replicas of particles which refers to the Trotter slices [15]. There is a set of harmonic springs with frequency ω_P accounts for the forces between copies. The related theory and techniques of PIMD are discussed in

previous studies [18, 16, 14, 12]. Considering only the translational kinetic and potential contributions, the discretized Hamiltonian referred to the P copies of a single quantum particle of mass m system moving in a potential $V(q)$ is given by [3]

$$H_P = \sum_{t=1}^{P} \left\{ \frac{p_t^2}{2P\tilde{m}_t} + \frac{1}{P}V(q_t) + \left(\frac{Pm}{2\beta^2\hbar^2}|q_t - q_{t+1}|^2 \right) \right\} \tag{2.1}$$

where p_t and q_t is, repectively, the fictional momentum attributed to the tth bead and the tth bead position, and $V(q_t)$ is the fictional external potential of tth bead. $\tilde{m}_t$ denotes an arbitrary mass of bead with $\tilde{m}_t = m/P$.

In terms of the corresponding estimator used in this method, both the primitive estimator and the centroid virial estimator are selected to measure the observables during the simulations, more details can be found in the related literature [47, 3].

Due to the stiff harmonic springs between the particle copies, the molecular dynamics method generates inefficient and nonergodic dynamics. Briefly, according to the discretized Hamiltonian, the external potential allows the energy exchange with the harmonic term. At a low temperature limit, the dynamics may fall into the so-called KAM regime and the non-ergodic problem may arise [48]. However, as the temperature or P increases, the force constant of the harmonic term also grows larger which leads to a stiffer harmonic

spring whereas the potential $V(q_t)/P$ becomes lower. Finally, it still causes an inefficient decorrelated or non-ergodic problem [48].

To circumvent the above difficulties, previous studies applied the thermostats to the PIMD method and successfully generated the ergodic, canonical results [16]. In this thesis, we use PIMD with PILE thermostat for sampling the translational part of the quantum system, which is already implemented in MMTK and benchmarked by previous studies [3, 4]. Also, we perform traditional PIMC for the simulation of rotation. As for the translational motion, MD can provide a system move with a movement of the center of mass of particles. Another reason to use MD more than MC in translational motion is that MD performs a real-time simulation by allocating the velocities and time steps in the "universe". However, MC only accounts for arbitrary steps, which lacks the information about motions and trajectories in real-time dimension.

However, we choose MC to implement rotational motion because of the shortcomings of mathematical generalization for rotation in PIMD. Then, we will introduce our MC algorithm for simulation of the rotational part in the following sections.

2.2 Direct Monte Carlo Integration: Classical System

Besides of quantum Monte Carlo method, we can first implement the direct Classical Monte Carlo Method (dCMC) method to test for the classical system.

According to Born-Oppenheimer (BO) approximation in a molecular system, the motion of atomic nuclei and electrons can be separated, and the electronic energy now is the function of nuclei position $\mathbf{R}$ and relative orientation $\mathbf{\Omega}$ which gives the potential energy surface (PES). Moreover, a further approximation is applied to molecules, the rigid-rotor approximation assuming molecules have fixed internuclear distance $\mathbf{r}$ for rotational motion. Moreover, in classical limit, the kinetic and potential part of partition function are separable, $z_{\text{int}}(T) = z_{\text{vib}}(T)z_{\text{rot}}(T)z_{\text{el}}(T)$. Based on these two approximations, we can have a total internal energy as a sum of all components: $E_{\text{int}} = E_{\text{vib}} + E_{\text{rot}} + E_{\text{el}}$. If we only consider the rotational contribution and ignore the vibrational motion, the internal energy is expressed as $E_{\text{int}} = E_{\text{rot}} + E_{\text{el}}$.

In classical mechanics, the formulation for rotational partition function of a single molecule can be evaluated as

$$z_{\text{rot}}(T) \approx \frac{2Ik_BT}{\hbar^2} = \frac{T}{\sigma\Theta_{\text{rot}}} \tag{2.2}$$

where σ is the symmetry number, and for N-particle, we have $Z_{\text{rot}}(T) = [z_{\text{rot}}(T)]^N$. Also, in classical limit, the rotational contribution with a rotational degree of freedom, f_{rot}, to the internal energy is generally

$$E_{\text{rot}}(T) = \frac{f_{\text{rot}}}{2} N k_B T \tag{2.3}$$

As for the electronic component or potential part of the partition function, in general,

$$z_{\text{pot}}(T) = \sum_{\text{states}} e^{-\beta \epsilon_{\text{states}}} \tag{2.4}$$

$$V(\mathbf{\Omega}) \equiv E_{el} = \frac{\sum_{\text{states}} \epsilon_{\text{states}} e^{-\beta \epsilon_{\text{states}}}}{z_{\text{pot}}} \tag{2.5}$$

In order to calculate the total internal energy, the main challenge is to evaluate the ensemble average for potential energy in thermodynamic equilibrium. According to the statistical mechanics, we know after a long time simulation, the system can reach thermodynamic equilibrium and the time average is equivalent to the thermodynamic average.

Therefore, it is possible to sample for the orientational configuration of all molecules in each Monte Carlo step and calculate the total potential energy for each step. After looping over all Monte Carlo step, the partition function and potential average can be calculated from the average over MC step.

From the above expression of the partition function, we can have the related classical thermodynamics information. Thus, the dCMC code can be implemented as follows,

Algorithm 1: Direct Classical Monte Carlo Integration (dCMC)

for $i <$ MC step **do**
  generate a set of random Euler angles $\{\mathbf{\Omega}\}$ for all molecules as a whole orientational configuration;
  calculate the potential energy $V_{\text{total}}(\mathbf{\Omega})$ for this configuration;
  calculate the numerator of the ensemble average potential energy $\langle V \rangle$ by multiplying the Boltzmann factor $V_{\text{total}}(\mathbf{\Omega}) * e^{-\beta V_{\text{total}}(\mathbf{\Omega})}$;
  calculate the partition function Z_{pot} by $Z_{\text{pot}} = \sum_i e^{-\beta V_{\text{total}}(\mathbf{\Omega})}$;
end
sum over the numerator of the ensemble average potential energy $\langle V \rangle$ by all Monte Carlo step;
calculate the ensemble average potential energy $\langle V \rangle$ by dividing by the partition function Z_{pot} which referred as $\langle V \rangle = \sum_i V_{\text{total}}(\mathbf{\Omega}) * e^{-\beta V_{\text{total}}(\mathbf{\Omega})} / Z_{\text{pot}}$;
calculate the total internal energy by adding up the classical rotational energy $E_{\text{rot}} = f_{\text{rot}}/2 * k_B T$ as $E_{\text{int}} = \langle V \rangle + E_{\text{rot}}$;

dCMC algorithm is efficient and able to extract both the thermodynamic and structural information of particles, we can use it for our system in the classical region.

2.3 Path Integral Monte Carlo: Metropolis-Hastings Algorithm

Traditionally, the Quantum Monte Carlo method [18] has been the tool to simulate molecular systems. Metropolis sampling is one of Markov chain Monte Carlo algorithm that can be used for N rotors with P beads under canonical ensemble system which is already developed by previous studies [45, 66], here is just a simple application for that algorithm

in our hybrid MD/MC code. The main algorithm is,

Algorithm 2: Modifed Metropolis-Hastings Algorithm in this thesis [45, 66]

```
acceptratio = 0;
for i < MC step do
    for a < N do
        for t_1 < P do
            the previous one t_0, and the latter one t_2;
            calculate the density operator element ρ_old and energy estimator for this
             configuration M_old by linear interpolation;
            move this bead t_1 by a random number based on orientation parameters
             and construct a new configuration M_new;
            calculate the density operator element ρ_new and energy estimator for the
             new configuration by linear interpolation;
            calculate the ratio of the probability and Boltzmann factor between the
             two configurations by P_accept = (ρ_new/ρ_old) e^{-τ(E_new - E_old)};
            if P_accept > 1.0 then
                accept, acceptratio+ = 1;
            else if P_accept ∈ rand then
                accept, acceptratio+ = 1;
            else
                reject;
            end
        end
    end
end
acceptratio/ = (MC step∗N ∗ P);
```

where ρ is a rotational density matrix element, E_{new} is the potential energy of the new configuration, E_{old} is the potential energy of the old configuration. In line 6 and line 8, the density matrix element values are calculated by the linear interpolation method based on the pre-calculated density matrix for a truncated energy level as a function of tabulated Euler angles.

The Monte Carlo movement will be accepted if the $\mathbf{P_{accept}}$ is larger than 1.0 which means the whole system has lower energy than the previous one. However, if we only accept the movement based on the energy change, the energy of samples will be trapped in the local energy minimum and it cannot be a "real" sampling since sometimes the energy may have to jump an energy gap to reach a global minimum. Therefore, if the energy of the new configuration is larger than the previous one, we have to calculate the Boltzmann factor, then generate a random number **rand** based on the continuous uniform distribution of $(0.0, 1.0)$. If the $\mathbf{P_{accept}}$ is smaller than 1.0, the movement is conditionally accepted based on the random number and the total acceptance ratio, which is acceptratio in the pseudocode, is calculated. The acceptance ratio is controlled under $(0.3, 0.5)$ by previous studies and preliminary results. Otherwise, the move will be rejected and the configuration of the particle will stay as the initial step. In terms of energy calculation, the configuration at each step, whether it is changed or not, should be considered to calculate the whole average.

Monte Carlo algorithms involving trial moves for each particle are called local-update Monte Carlo Algorithms. However, this kind of local-update algorithm in the calculation of the equilibrium statistical mechanics has several disadvantages in essence.

A valid Monte Carlo method should obey two rules: detailed balance and ergodicity. The detailed balance of the Metropolis-Hastings algorithm [66] has been proved. But the local-update results may be trapped in an energy minimum point at a low temperature due to the probability distribution, which may lead to a non-ergodic simulation. Moreover, the temperature near to the critical point which is a continuous phase transition, T_c, will cause a so-called phenomenon "critical slowing down" [49]. The correlation time for the simulation will increase remarkably and be very difficult to generate an independent configuration. Thus, new algorithms for Monte Carlo methods are urged to conquer the non-ergodic problem and suppress the long correlation time.

2.4 Path Integral Monte Carlo: Cluster Monte Carlo Algorithms

2.4.1 Cluster Algorithm: Lattice System

New cluster-update algorithms were developed by Swendsen and Wang (SW) in 1987 [5] for the study of lattice spin flipping and magnetization, and also by Wolff in 1989 [6] for the study of a single-cluster algorithm using Ising Model. As both of the algorithms related to a cluster update of the whole system and a rejection-free process, the Wolff algorithm only considers a single-cluster formation and update, which has much better efficiency than Swendsen-Wang's. Furthermore, the effect of the "critical slowing down" on the simulation in Wolff's algorithm is much smaller than the previous one. This algorithm has been modified and updated by Sierens et al in 2017 [50] for the lattice spin system with on-site interactions, which expands this algorithm to an interacting system.

$$\hat{H}_{\text{spin}} = \hat{H}_{\text{n.n.}} + V^i \tag{2.6}$$

$$\hat{H}_{\text{n.n.}} = -J \sum_{ij} \mathbf{n_i} \cdot \mathbf{n_j} \tag{2.7}$$

where n_i is the spin at site i, V^i is the potential interaction on site i (for example, an on-site magnetic field $\mathbf{B}_i$). In the original Wolff's algorithm, the link probability $\mathbf{P_{link}}$, which controls the growth of the cluster, depends on the nearest-neighbour coupling energy of spins referred to $\hat{H}_{\text{n.n.}}$. In the presence of the external field, the previous algorithm can be modified by adding a cluster acceptance ratio, $\mathbf{P_{accept}}$. The cluster generated by $\mathbf{P_{link}}$ can only accept and flip with $\mathbf{P_{accept}}$.

$$\mathbf{P_{accept}} = \min\{1, \exp(-\Delta E_{\text{on-site}}/T)\} \tag{2.8}$$

$$= \min\left\{1, \exp\left[-\frac{1}{T}\sum_{i\in\text{cluster}}(V^{i'} - V^i)\right]\right\} \tag{2.9}$$

where V^i is the potential interaction on site i before flipping, and $V^{i'}$ is the potential interaction on site i after flipping.

Thus, the modified Wolff's algorithm for this system is shown as follows.

Algorithm 3: Modifed Wolff's Algorithm for spin system with on-site interaction [50].

A spin **i** is selected at random;
add site **i** to the cluster, **clu**, and to the buffer, **buf**;
while the **buf** is empty **do**
    pop the site **i** off **buf**;
    adding all neighboring spins **j** to the **clu** and **buf** with a probability $P_{link} = 1 - \exp(2\beta J)$;
end
calculate the acceptance probability, $\mathbf{P_{accept}}$;
for i $\in$ ***clu*** **do**
    reflect $\mathbf{n_i}$ about the hyperplane orthogonal to random vector **v** such that $\mathbf{n_i} \rightarrow R(\mathbf{v})\mathbf{n_i} = \mathbf{n_i} - 2(\mathbf{v}\cdot \mathbf{n_i})\mathbf{v}$;
end

where $\mathbf{n_i}$ is the unit vector representing the spin i, **v** is a random unit vector as a reflection reference, and $R(\mathbf{v})$ denotes the reflection transformation about vector **v**.

2.4.2 Cluster Algorithm: Continuum Systems

As the advantages of the cluster-update algorithm introduced previously, a wide application on the continuum systems such as translational particles is pursued to implement. In 1995, Dress and Krauth achieved a method to generate particle configurations for a hard-sphere

system including only repulsive interaction, which is so-called Geometric Cluster Algorithm (GCA). Furthermore, a generalized GCA for interacting particles including both attraction and repulsion is also suggested by them and introduced by E. Luijten et al [49].

Algorithm 4: Generalized Geometric Cluster Algorithm for Interacting Particles [7].

1 A 'pivot' $\mathbf{v}$ is selected at random in a given configuration $\{C\}$;
2 A particle i at position $\mathbf{r}_i$ is selected as the first particle that added to the cluster, $\mathbf{c}$;
3 This particle i is moved via a point reflection with respect to the pivot, $\mathbf{v}$. In its new position, the particle is referred to as i', at position $\mathbf{r}'_i$;
4 adding all interacting particles j with i or i' to the $\mathbf{c}$ with link probability $p_{ij} = \max[1 - \exp(-\beta\Delta_{ij}), 0]$, where $\Delta_{ij} = V(|\mathbf{r}'_i - \mathbf{r}_j|) - V(|\mathbf{r}_i - \mathbf{r}_j|)$;
5 add j also to the stack $\mathbf{s}$;
6 **while** $\boldsymbol{s}$ is not empty **do**
7 a particle is retrieved from the stack $\mathbf{s}$ as a new "i" in step 2;
8 repeat step 4 and step 5;
9 **end**

Since the previous studies for the cluster-updates Monte Carlo method are limited to the classical system, potential implementation of this algorithm to a quantum rotational system with path integral formulation is introduced and tested in this thesis.

Chapter 3

Benchmark: Finite Temperature Path Integral Monte Carlo Method

3.1 PIMC proof of principle: linear top system HF monomer with Electric Field along z-axis

Since we will implement all the PIMC source code with MMTK package and test the hybrid PIMD and PIMC later, the first step is to benchmark the local-update PIMC code for both linear and asymmetric top systems and confirm the validity and accuracy of various quantum systems. The related energy and structural information are also computed in this part with a quadratic convergence of energy versus τ as mentioned in the theory chapter. The later study of the cluster-update Monte Carlo method is also based on the results of this part. As the first test, a linear top system is tested with Hydrogen Fluoride monomer in an electric field. The PIMC simulation tests have been completed with a linear density

matrix generator written in Fortran 77 [51].

3.1.1 System Setup

A simple HF monomer system is constructed to test the PIMC code for a linear system. Since the diagonalization of the rotational operator with the electric field along the z-axis ($\mathbf{E}_z$) can be calculated directly, the PIMC results can be benchmarked against an exact sum-over-states result. The detailed derivation of the diagonalization of the rotational operator with $\mathbf{E}_z$ field is attached in Appendix A.1., and the Hamiltonian of this system is

$$\hat{H} = \hat{T}_{\text{rot}} + V(\theta) \tag{3.1}$$

where $\hat{T}_{\text{rot}}$ is the rotational operator, $V(\theta)$ is the potential function in the electric field along z-axis, and θ here denotes the angle between linear rotor HF and z-axis.

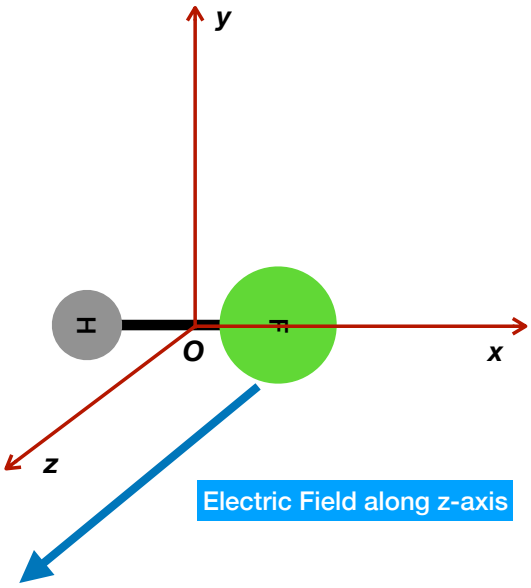

Figure 3.1: HF monomer placed along x-axis in an electric field along z-axis

Shown in Figure 3.1, the center of mass of this HF molecules is placed at origin and the whole molecule is along the x-axis, with an electric field applying along z-axis. The parameters is shown in Table 3.1.

3.1.2 Results

As introduced in theory part, an accurate result can be obtained by a convergence study with different τ. The simulation is computed with various number of P ranging from 8 to 128. A quadratic fit and the exact diagonalization result are shown in Figure 3.2, with

Table 3.1: The Parameters for the Simulations of HF monomer

Parameters	Values
Temperature (T, K)	5.0K
Rotational Constant (B, cm^{-1}) [52]	20.9557
Electric Field Strength $(E, \mathrm{V/m})$	1.0×10^8
Simulation Step	2000000
Simulation Skip Step	200.0
Number of Beads (P)	$[8, 16, 32, 64, 128]$
Acceptance Ratio	$(0.3, 0.5)$
Density Grid Points	150000

standard errors for each simulation data point.

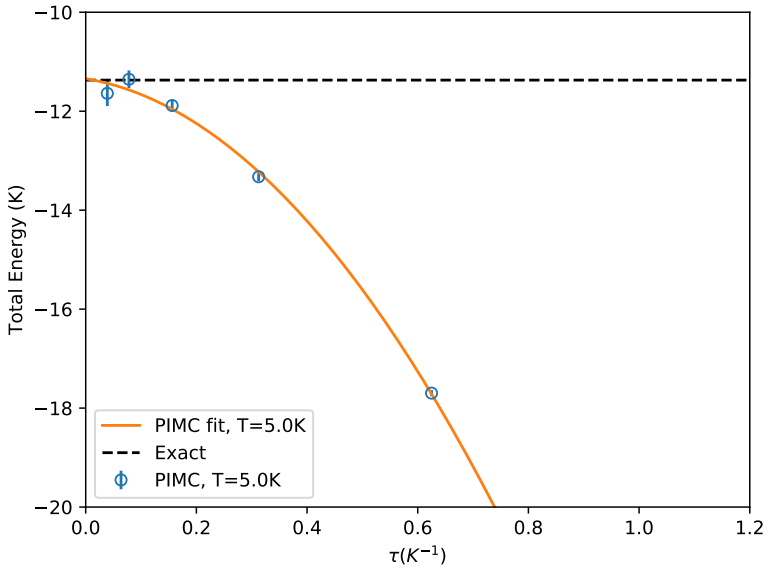

Figure 3.2: Convergence of the PIMC Total Energy of the HF monomer with respect to τ for $T = 5.0$ K. A quadratic fit to the data is shown as a solid line. The exact value obtained from explicit diagonalization is shown as a dashed line.

A clear quadratic relationship can be found in the total energy convergence plot versus τ. When the τ reach around 0.001 to 0.002 K^{-1}, the energy obtained from PIMC is within 2.3% of the exact value. Moreover, the structural information can also be analyzed in PIMC calculation. The angular distribution for the angle between HF rotor and z-axis is shown in Figure 3.3.

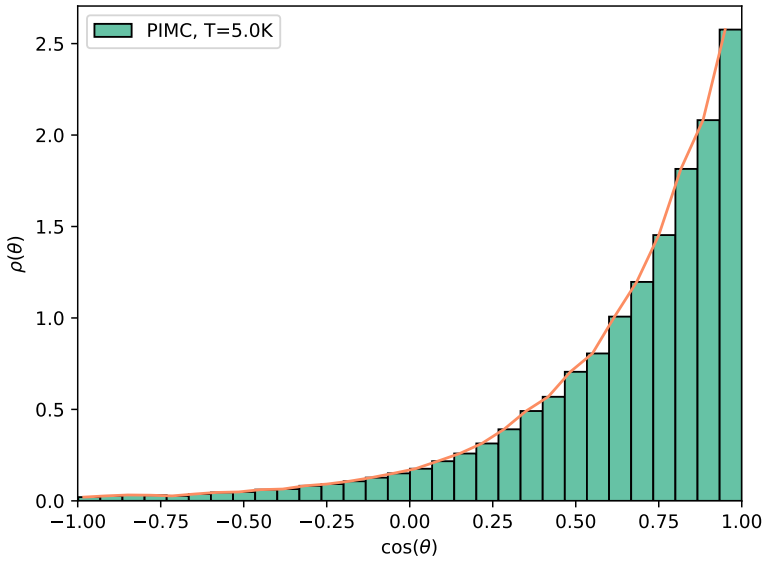

Figure 3.3: Angular distribution of $\cos(\theta)$ for $T = 5.0$ K at $\tau = 0.0015625$ K^{-1}

.

The trend of the angular distribution plots indicate a preference for HF molecule parrallel to the z-axis direction which matches the behaviour of the electric dipole in the electric field.

3.2 PIMC proof of principle: asymmetric top system H_2O Dimer Simulation

Having benchmarked linear top PIMC code, the next step is to implement asymmetric top PIMC code in the MMTK package. Since the MMTK package can track the Cartesian coordinates information of molecules, we need to determine and fill the Euler angles for the rotation matrix of asymmetric top especially C_{2v} symmetry for water from the inertia of tensor. The detailed derivation of Euler angles calculation is attached in Appendix A.2, and the related Euler angles definition is also explained there. First of all, a water dimer system is considered to be simulated for a high temperature system with both dCMC and PIMC. Water molecules are treated as fixed and rigid rotors which have a wide range of lattice spacing between the center of mass. Also, a developed analytical water model such as Quantum Simple Point Charge Flexible Water (q-SPC/FW) [53] Quantum Transferable Intermolecular Potential with 4 Points Flexible (q-TIP4P/F) [54, 55] is used to describe the interactions for water system. It is noted that a more accurate many-body force field should be applied to these systems like Many Body - Polarizable (MB-Pol) model [56, 57, 58], but the expensive computing efforts for the calculation of the potential part should also be considered. Based on the balance of accuracy and efficiency, we chose q-TIP4P/F as our

first model to test the following water system.

3.2.1 System Setup

As shown in Figure 3.4, two water molecules are separated by a fixed lattice spacing and placed along z-axis.

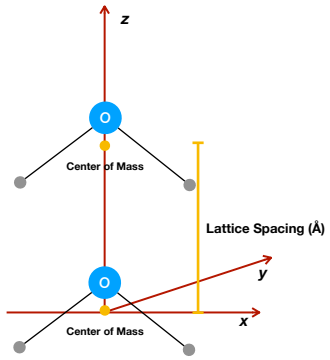

Figure 3.4: Water dimer placed along z-axis

The Hamiltonian for this water dimer system can be expressed as

$$\hat{H} = \hat{T}_1^{\text{rot}} + \hat{T}_2^{\text{rot}} + V(\mathbf{\Omega}_1, \mathbf{\Omega}_2) \tag{3.2}$$

where $\hat{T}_i^{\text{rot}}$ represents the rotation of rigid water molecule i, and $V(\mathbf{\Omega}_1, \mathbf{\Omega}_2)$ represents the potential between two water molecules in the orientation representation $\mathbf{\Omega}_i =$

$\{\varphi_i, \theta_i, \chi_i\}$.

The related detailed calculation parameters used in our codes are shown in Table 3.2 and Table 3.3. The number of beads $P = 2$ is chosen for the simulation in PIMC at a very high temperature which indicated a "nearly classical" system, and the results will be compared with dCMC code. All the simulation step and simulation skip step (which is necessary in PIMC code for a decorrelated process) is determined by preliminary tests for this system.

Table 3.2: The Parameters for the Simulations of Water Dimer with PIMC method

Parameters	Values
Temperature (T, K)	$(20.0, 300.0)$
Rotational Constant ($A, B, C, \mathrm{cm}^{-1}$) [59]	27.8761, 14.5074, 9.2877
Simulation Step	400000
Simulation Skip Step	100.0
Number of Beads (P)	[2]
Acceptance Ratio	$(0.3, 0.5)$

Table 3.3: The Parameters for the Simulations of Water Dimer with dCMC method

Parameters	Values
Temperature (T, K)	$(20.0, 300.0)$
Rotational Constant (A, B, C, cm^{-1}) [59]	27.8761, 14.5074, 9.2877
Simulation Step	1000000

3.2.2 Results

For a high temperature as 300.0 K, PIMC matches perfectly with dCMC for a range of the lattice spacing from the repulsive part to attractive region, and also the non-interaction region. It can also be seen that in the minimum point, there is a larger discrepancy in the total energy between PIMC and dCMC.

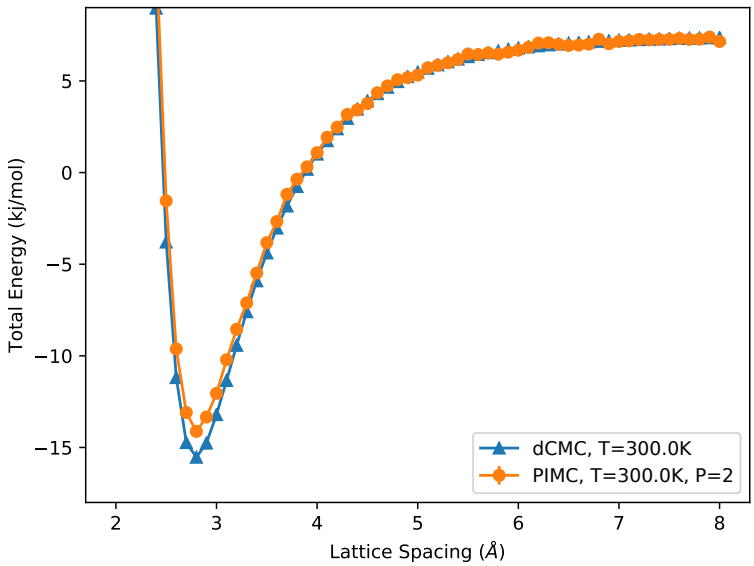

Figure 3.5: Total energy of water dimer at $T = 300.0$ K as a function of lattice spacing for q-TIP4P/Fw

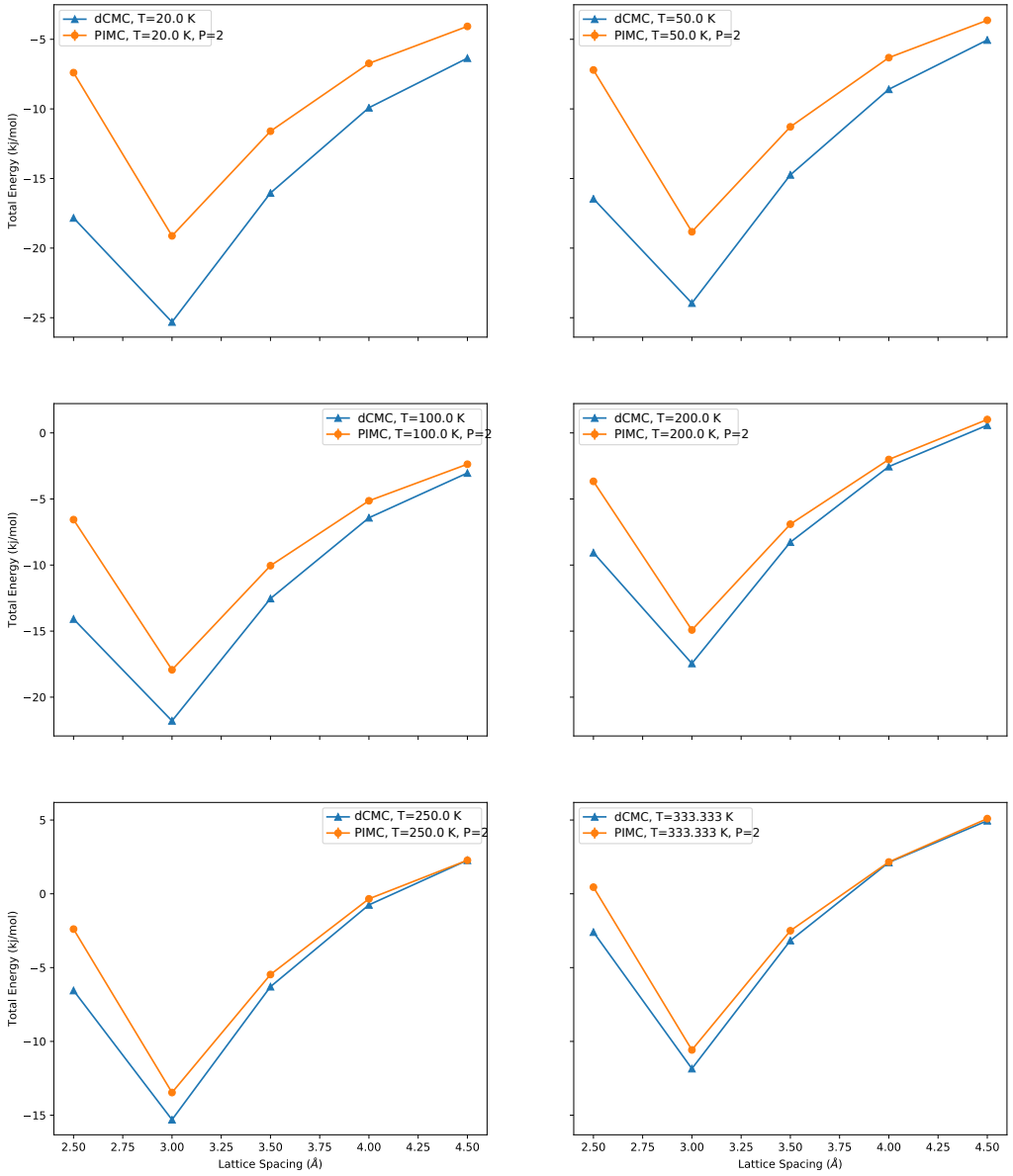

Figure 3.6: Total energy of water dimer at different temperature as a function of lattice spacing for q-TIP4P/Fw

We also perform the simulations with various lattice spacing around minimum total energy for various temperatures. From Figure 3.6, it indicates that dCMC and PIMC reach a better agreement at high temperature and also at larger lattice spacing. There is a large discrepancy between two methods around the minimum point and also the same for low temperature where may have more quantum effects and the number of beads $P = 2$ is not enough to generate converged and accurate results.

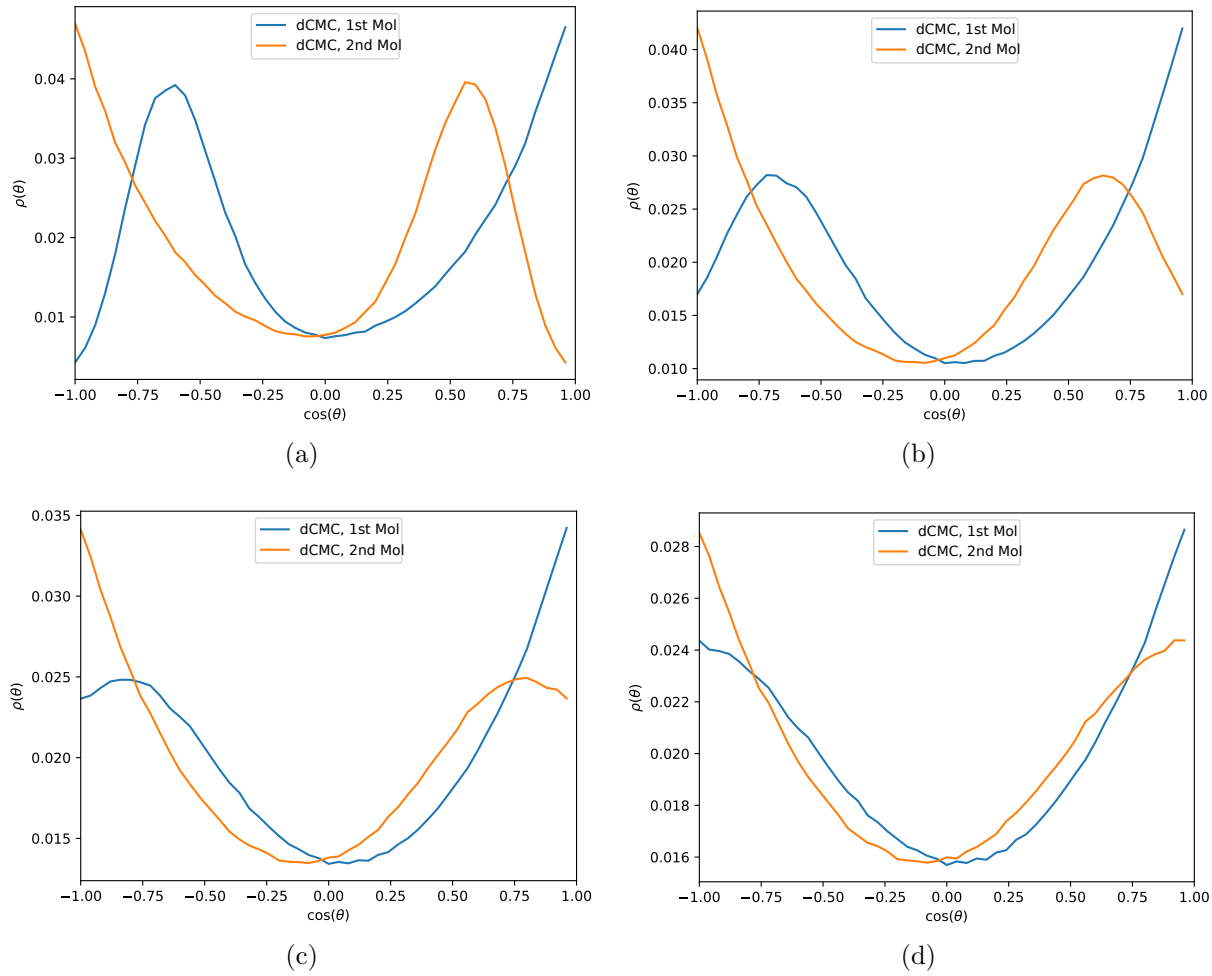

Figure 3.7: Angular distribution of water dimer by DMC simulations at $T = 300.0$ K for different lattice spacing (a) $R = 3.0$ Å (b) $R = 3.5$ Å, (c) $R = 4.0$ Å, (d) $R = 4.5$ Å. The blue line is for the first water molecule, and the orange line is for the second one.

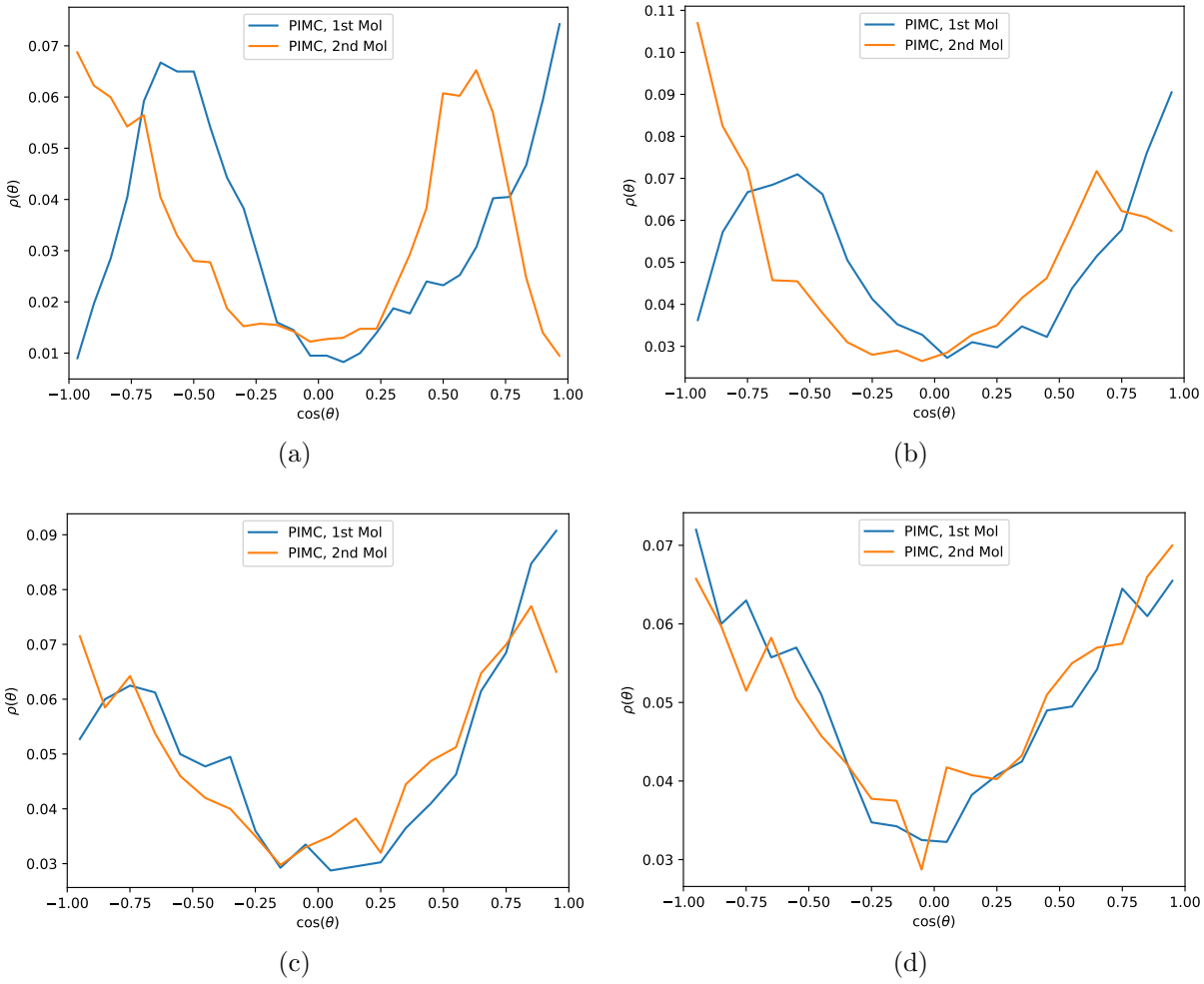

Figure 3.8: Angular distribution of water dimer by PIMC simulations at $T = 300.0$ K for different lattice spacing (a) $R = 3.0$ Å (b) $R = 3.5$ Å, (c) $R = 4.0$ Å, (d) $R = 4.5$ Å. The blue line is for the first water molecule, and the orange line is for the second one.

From the angular distribution plots from both dCMC and PIMC calculations, an angular distribution with less noises for a single dCMC simulation is about 30 seconds, however, the PIMC takes about one hour to complete the simulation under the same conditions.

A longer decorrelation time and also a longer simulation time are required to reach the converged status for the PIMC method which means that the PIMC is less efficient than the dCMC method at high temperature. Even if the energy and thermodynamic results are close enough, the structural results may also differ. This suggests that if we need to predict the structural information of molecules at high temperature with less computational expenses, dCMC can be used to predict the behaviour of molecules in the classical limit. noise can be found in the PIMC results which indicates a non-converged calculation.

Chapter 4

Application: Prediction of 1D Water Chain Behaviour and Phase Transition at Finite Temperature

4.1 Introduction

As introduced in Chapter 1, quantum confined molecules aroused scientists' great interests especially the 1D water chain confined in SWCNT. This chapter will explore one of the applications of dCMC calculations on a 1D water chain at finite temperature. For simplicity, the CNTs are not included in this thesis, and we start with exploring the behaviour of a pure water chain with only many water molecules interactions. Since a wide range of temperatures will be tested from around 15.0 K to 300.0 K, if β is too small, even in the $\tau \to 0$ limit, the converged correct energy and structural distributions can not be

obtained from PIMC calculation. We will perform dCMC code at first to cover all ranges of temperatures for classical calculations to analyze the energy and structural results.

4.2 System Setup

The 11 water rotors are placed along z-axis with the lattice spacing between the center of mass for each molecule fixed. Figure 4.1 displays the scheme of the system we used in the simulations.

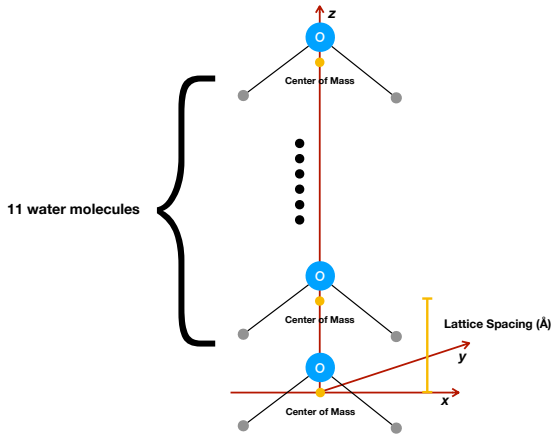

Figure 4.1: 11 Water rotors placed along z-axis

Since we want to explore the behaviour of the 1d water chain, a wide range of temperatures from 15.0 K to 300.0 K is used. Moreover, the lattice spacing also a significant factor of water interactions, a variety of lattice spacing from 2.5 Å to 5.0 Å is considered.

And we perform these systems with only dCMC code, the related parameters are shown in Table 4.1.

Table 4.1: The Parameters for the dCMC Simulations of 11 Water Rotors as a chain

Parameters	Values
Temperature (T, K)	$(15.0, 300.0)$
Rotational Constant (A, B, C, cm^{-1}) [59]	27.8761, 14.5074, 9.2877
Simulation Step	1000000

From the preliminary tests of the dCMC simulation for water chain system, an acceptable MC simulation step of 1000000 is chosen in the whole set of simulations determined by the balance of accuracy and effciency.

4.3 Results

In order to explore the orientational behaviour of 1D water chain, there are several order parameters are chosen for the related measurements. A nearest neighbouring orientational correlation of molecular dipole moments is defined as $\boldsymbol{\mu}_i\boldsymbol{\mu}_{i+1}/||\boldsymbol{\mu}||^2$, which is the dot product between the nearest neighboring molecules' dipoles. $\boldsymbol{\mu}_i$ denotes the vector representation for the dipole moment of the water molecule i, and $||\boldsymbol{\mu}||$ is defined as the magnitude of the dipole moment. Also, we sum over the nearest neighbour orientational correlation function for each molecule and divided by the total number of molecules used

in the calculation. In our simulation, we have 11 water molecules but only the middle 7 water molecules are calculated for the orientational measurement to avoid the end effect. Thus, we have $\sum_i^{N-1} \boldsymbol{\mu}_i \boldsymbol{\mu}_{i+1}/(N||\boldsymbol{\mu}||^2)$. Similarly, we also calculate the related measure for the corresponding z-component nearest neighbour orientational correlation dipole moments, $\mu_i^z \mu_{i+1}^z/||\boldsymbol{\mu}||^2$. Besides of the correlation function, the orientational behaviour for each single water molecule is also measured by the mean normalized magnitude of the perpendicular dipole component for one water molecule, $||\boldsymbol{\mu}_\perp||/||\boldsymbol{\mu}||$, and the z-component $||\boldsymbol{\mu}_z||/||\boldsymbol{\mu}||$. All measurements above are finally take the sum of the middle 7 molecules, and do the average over the total number of measured molecules 7.

From the Figure 4.2, we can find two significant transitions around 3.1 Å and 3.9 Å for all orientational measurements.

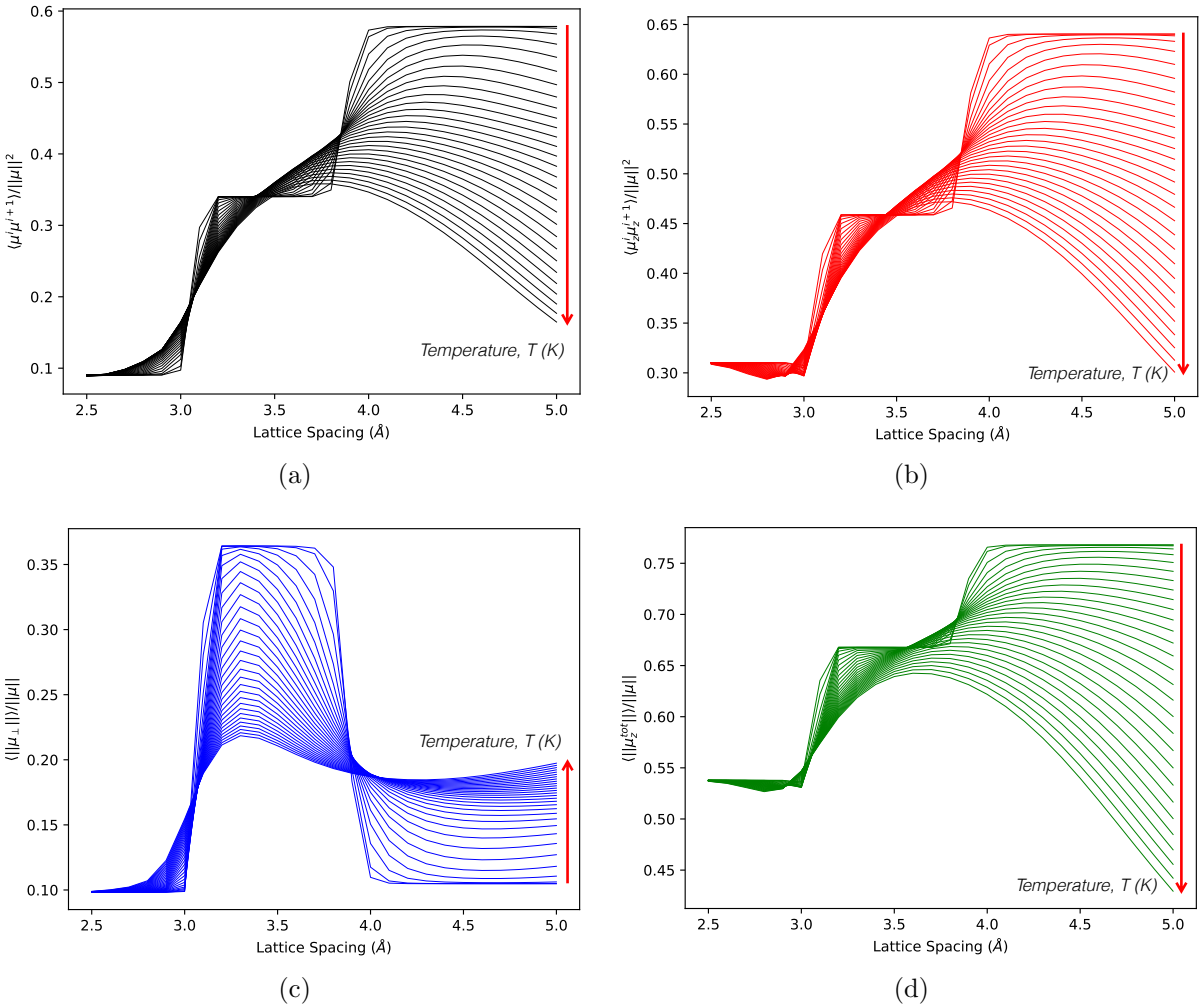

Figure 4.2: (a) Nearest neighbouring orientational correlation of molecular dipole moments and (b) related measure for the components parallel to the z-axis. (c) mean normalized magnitude of the perpendicular dipole component for one water molecule (d) mean normalized total dipole moment along the z-axis. All measurements are averaged over central 7 molecules, and the red arrow denotes the temperature goes from low to high.

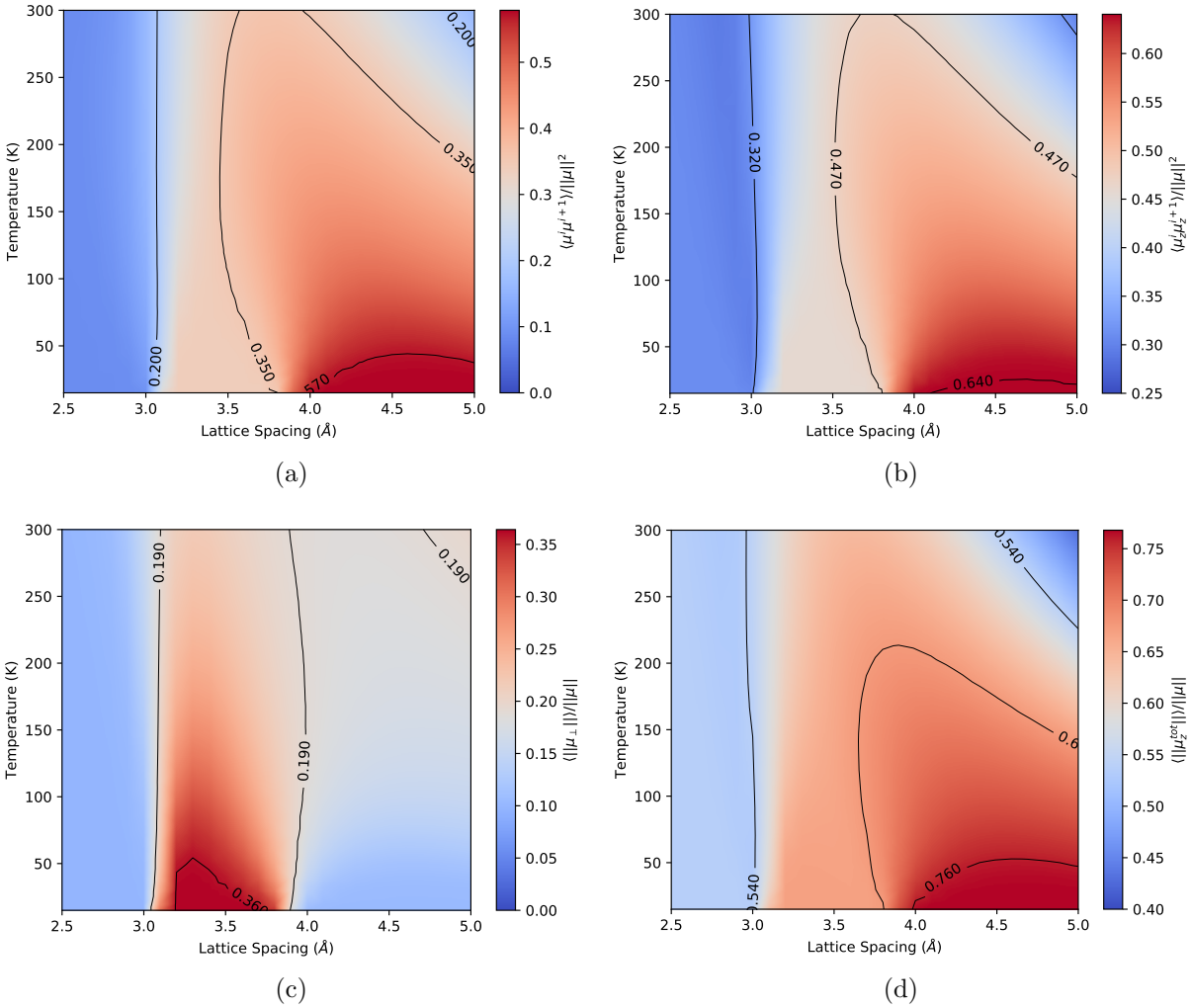

Figure 4.3: Phase transition plots based on different order parameters (a) nearest neighbouring orientational correlation of molecular dipole moments and (b) related measure for the components parallel to the z-axis. (c) mean normalized magnitude of the perpendicular dipole component for one water molecule (d) mean normalized total dipole moment along the z-axis. All measurements are averaged over central 7 molecules.

Then, we can obtain the phase transition plots from the orientational measurements. Since the classical hydrogen bonding has a preference of 31° angle about the z-axis, and the

dipole-dipole interaction has a preference of parrallel along the z-axis. The temperature-lattice spacing phase plot can be divided into three regions, the first region is before 3.1 Å. In this region, there is a low nearest neighbor correlation and also a low dipole moment for both perpendicular and parrallel to z-axis component, which indicate a disorder and decorrelated region due to high repulsive interactions and a broken hydrogen bonding. The second region is between 3.1 Å and 3.8 Å where it has a relatively high nearest neighbouring correlation, and also high dipole moment for both perpendicular and parrallel component dipole. It presents a highly ordered structure which is due to the hydrogen bonding between water molecules. The third region is located after 3.8 Å lattice spacing, a higher correlation suggests a more correlated interaction is dominant. Also, a more z-component but less perpendicular component dipole moment indicates a dominant parrallel structure between water molecules which is due to the long-range dipole-dipole interactions. Therefore, the three region can be divided as "repulsive region", "hydrogen bonding region", and "dipole-dipole region".

Chapter 5

Hybrid PIMD/PIMC Methods Preliminary Test

Having implemented PIMC code and PIMD code in the MMTK package and proved the validity of the PIMC code in the previous chapters. This chapter now will turn to a more complicated hybrid PIMD/PIMC method with a linear rotor in a soft superfluid solvent including both translational and rotational motion: CO_2 doped Helium. The Hamiltonian for this system can be written in the following form:

$$\hat{H} = \hat{H}_{CO_2} + \hat{H}_{He} + V_{CO_2-He}(\mathbf{R} - \mathbf{r}_i, \mathbf{\Omega}) \tag{5.1}$$

where $V_{CO_2-He}(\mathbf{R} - \mathbf{r}_i, \mathbf{\Omega})$ is the two-dimensional CO_2-He potential, and $\{\mathbf{R}, \mathbf{r}_i\}$ are, respectively, the center of mass of the CO_2 molecule and positions of the helium atoms. $\mathbf{\Omega}$ is the orientation of the molecule in MFF.

$$\hat{H}_{\mathrm{CO_2}} = B\hat{l}^2 + \frac{\hat{P}^2}{2m_{\mathrm{CO_2}}} \tag{5.2}$$

$\hat{H}_{\mathrm{CO_2}}$ represents the rotational and translational degrees of freedom of the CO_2 molecule in the rigid rotor approximation, with $\hat{l}$ being the angular momentum operator and $\hat{P}$ the kinetic operator. B denotes the rotational constant of the CO_2 moleculle, $m_{\mathrm{CO_2}}$ is the mass of the molecule.

And the Hamiltonian for Helium atoms is

$$\hat{H}_{\mathrm{He}} = \sum_i \frac{\hat{p}_i^2}{2m_{\mathrm{He}}} + \sum_{i<j} v(|\mathbf{r}_i - \mathbf{r}_j|) \tag{5.3}$$

where $\hat{p}_i$ is the momenta of the helium atoms.

5.1 Hybrid PIMD/PIMC Algorithm

PIMD is performed on a real timescale (dt) which is related to molecular dynamics but PIMC is simulated with an imaginary timescale (β) for thermodynamics. Also the rotational correlation time, which is defined as the average time it takes for a molecule to rotate one radian, have a magnitude around $\tau_c = 1$ ps [60], and PIMD time step for translational motion is usually around $dt = 1$ fs. A new parameter, rotational skip step N_{rsk}, is necessary

to control how many translational steps should be run within one rotational step.

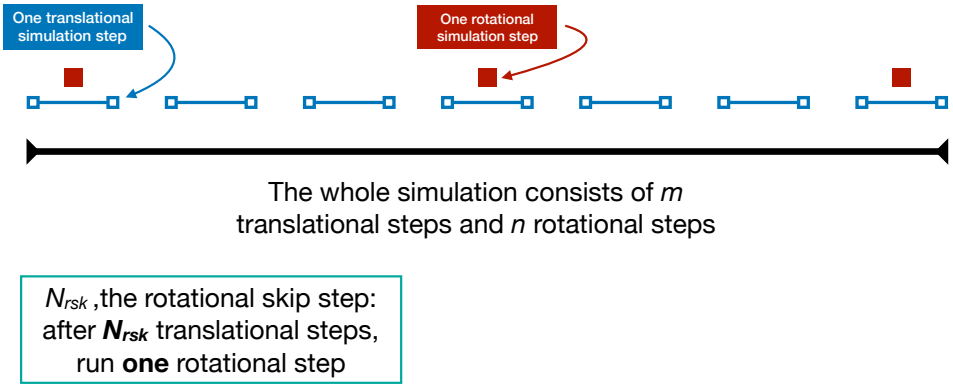

Figure 5.1: Illustration of the definition of the rotational skip step, N_{rsk}

However, the exact N_{rsk} should be determined by comparison with benchmark calculations. Since PIMC for CO_2-He system has been studied and proved, we will use the MoRiBS PIMC code [45] as a benchmark calculation for our new hybrid PIMD/PIMC

method.

Algorithm 5: Hybrid PIMD/PIMC Algorithm

```
for i < MD step do
    move the center of mass of the molecule by molecular dynamics calculation;
    calculate the primitive estimator for translational and potential energy;
    if MD step%N_rsk == 0 then
        for all beads and all molecules do
            rotate the molecule by a random angle and calculate
              P_accept = (ρ_new / ρ_old) e^{-τ(E_new − E_old)};
            if P_accept > 1.0 then
                accept;
            else if P_accept > rand then
                accept
            else
                reject
            end
        end
    end
    calculate the rotational and potential energy;
    calculate the acceptance ratio;
end
```

5.2 System Setup

The system setup sketch is shown in Figure 5.1, and the related parameters used in our simulations are shown in Table 5.1. Since we need to retain the superfluidity of the Helium atom, we chose 1 K as our test temperature. We test this new hybrid code with different P values for fixed temperature and rotational skip step, $N_{\text{rsk}} = 1$ at first to compare with MoRiBS PIMC code. Then, we will perform a parrallel comparison between all the same parameters but various N_{rsk} to explore the rotational skip step's effect on the final results.

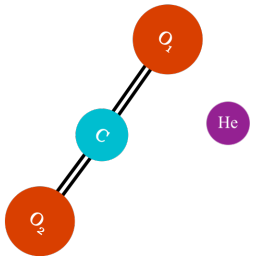

Figure 5.2: CO_2 doped with the single Helium atom

5.3 Results

As shown in Table 5.1, various number of beads are used to calculated the same CO_2-He system at $T = 1.0$K. It can be seen that the good match with pure PIMC code and low

Table 5.1: The Parameters for the Simulations of CO_2-He

Parameters	Values
Temperature (T, K)	1.0
Rotational Constant (B, cm^{-1}) [61]	0.39021
Simulation Step	500.0 ps/dt
Simulation Skip Step	100.0 fs/dt
Number of Beads (P)	$[8, 16, 32, 64]$
Acceptance Ratio	$(0.3, 0.5)$
Density Grid Points	150000

standard errors in our new hybrid PIMD/PIMC code for all kinds of energy, especially potential and translational energy.

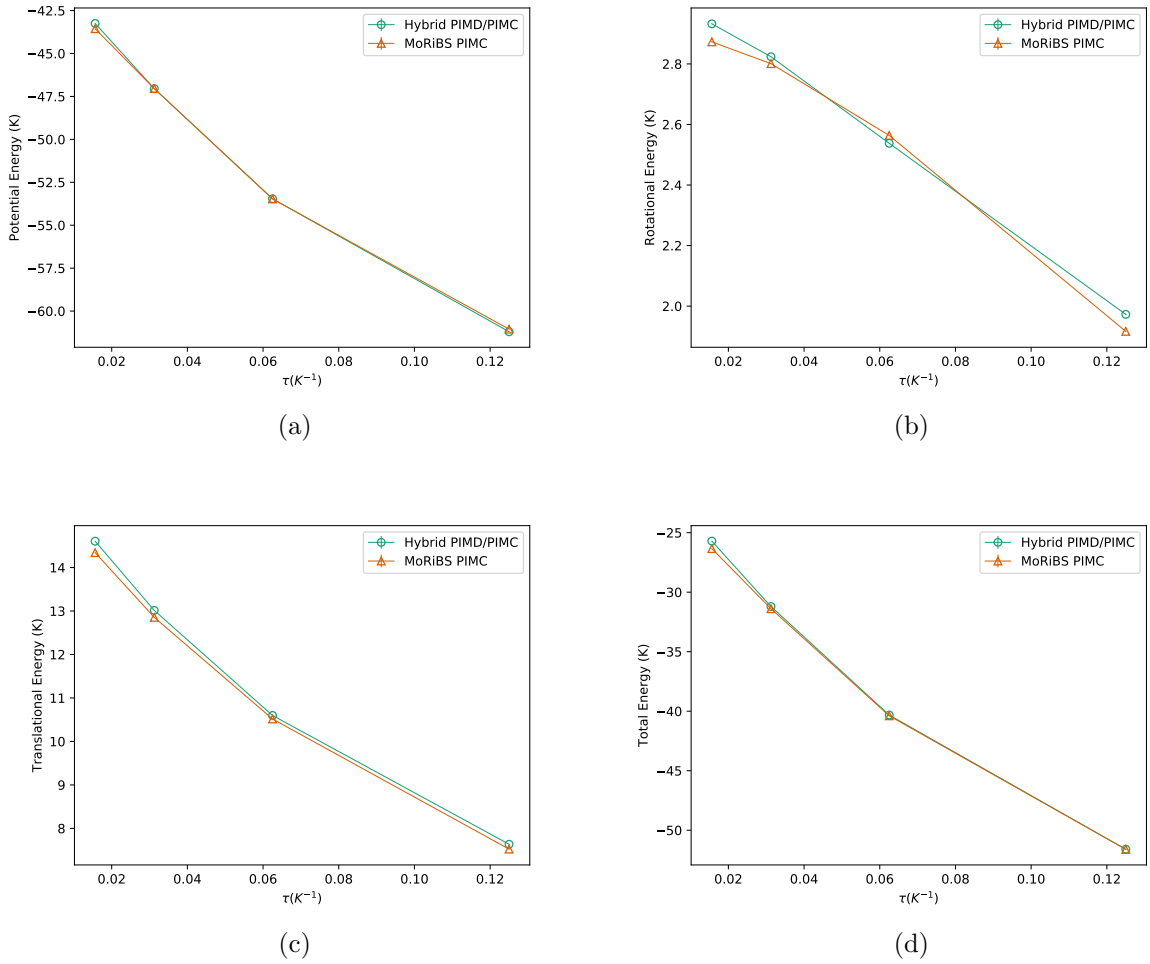

Figure 5.3: Hybrid PIMD/PIMC Simulations for CO_2-He at $T = 1.0$ K with $N_{\text{rsk}} = 1$ as a function of τ (a) potential energy (b) rotational energy (c) translational energy (d) total energy. The green data points with errobars are the hybrid PIMD/PIMC simulations' results, and the orange data points with errobars are the benchmarked MoRiBS PIMC results

There are small discrepancies in the rotational part, then a test for different N_{rsk} is needed to perform for the above system. Figure 5.3 shows that for rotational skip step

smaller than 20, there is a fluctuation for all kinds of energy around the result of pure PIMC, but the fluctuation may be due to the un-converged simulation, which indicates a longer simulation time or a longer decorrelated time. Furthermore, if the N_{rsk} is too large, both the translational and rotational energy will diverge from the correct value.

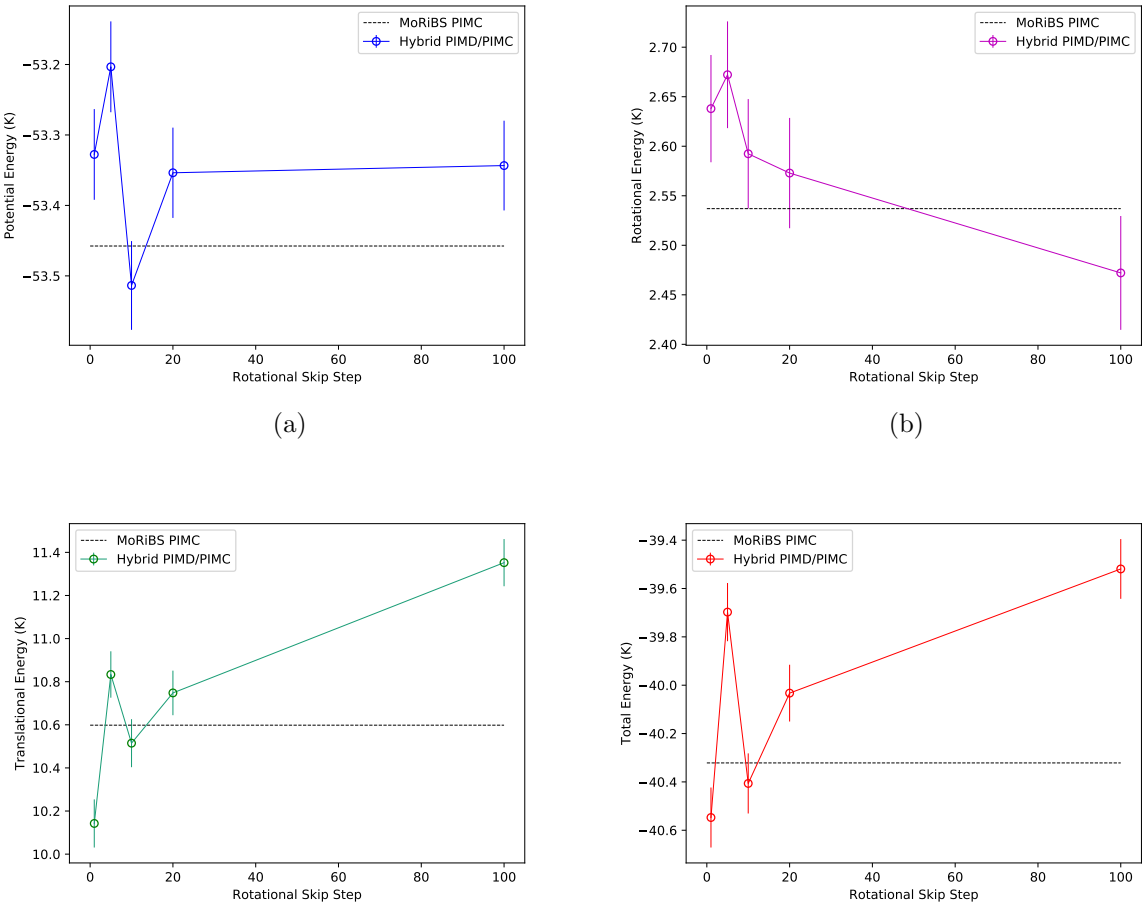

Figure 5.4: Hybrid PIMD/PIMC Simulations for CO_2-He at $T = 1.0$ K with $P = 16$ as a function of rotational skip step (a) potential energy (b) rotational energy (c) translational energy (d) total energy. The data points with errobars are the hybrid PIMD/PIMC simulations' results, and the black dashed lines are the benchmarked MoRiBS PIMC results

5.4 Concluding Remarks

We have successfully calculated the three energy components of CO_2-He system and our results agree with the pure PIMC calculation by MoRiBS. However, more complicated systems should be tested for this new hybrid code. Also, an energy convergence study and structural distribution should be done for this program to prove the advantages of our new code. We need a time-consuming comparison between the hybrid code and pure code to test the efficiency. As a result, we conclude that the hybrid PIMD/PIMC method works and practical.

Chapter 6

PIMC Cluster-update Algorithm Implementation

In the last chapter, we will explore the cluster-update algorithm for a quantum many-body rotational system with path integral formulation. Based on the previous calculations, there is a non-ergodic problem for the local-update algorithm while the cluster-update method can combat this issue. Based on the previous research of cluster-update, in this thesis, we focus on the GCA method since it is utilized for a continuum translational hard-sphere system [7, 49] which is similar to our continuum rotational system. The Hamiltonian of this system can be written as

$$\hat{H} = B\hat{l}^2 + \sum_{i<j} V(\mathbf{n}_i, \mathbf{n}, j) + \hat{H}_{beads} \tag{6.1}$$

where $\hat{l}$ represents the rotational operator, and B is the rotational constant. The second term can be in general the interaction between molecule $\mathbf{n}_i$ and molecule $\mathbf{n}_j$, the third term

represents the interaction between beads, P. And the dipole-dipole interaction analytical form is given by [62]

$$V(\mathbf{n}_i, \mathbf{n}, j) = \frac{d^2}{4\pi\varepsilon_0 r^3}(\hat{\Omega}_i \cdot \hat{\Omega}_j - 3(\hat{\Omega}_i \cdot \hat{r})(\hat{\Omega}_j \cdot \hat{r})) \tag{6.2}$$

where ε_0 is the vacuum permittivity, $\hat{\Omega}_i$ is the orientation unit vector of the molecule $\mathbf{n}_i$, r represents the distance between $\mathbf{n}_i$ and $\mathbf{n}_j$, and $\hat{r}$ represents the unit vector between dipoles.

Also, the visualization of this system can be described in Figure 6.1.

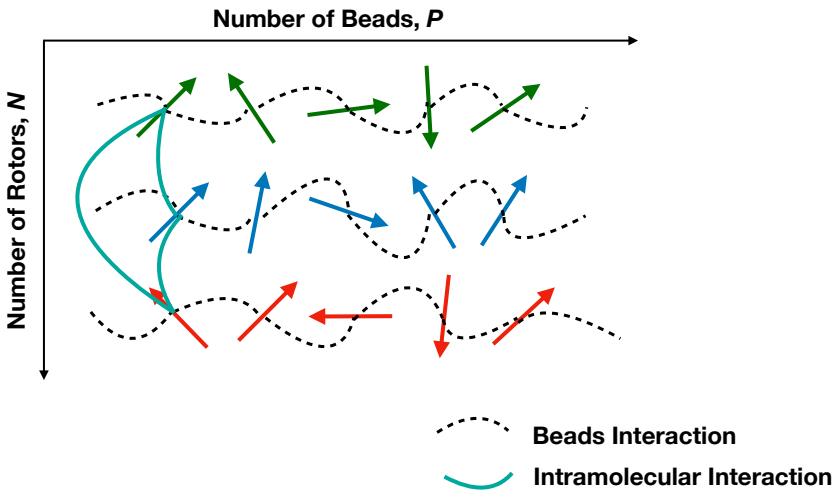

Figure 6.1: Illustration of the rotational dipoles in Path Integral formulation with intramolecular interactions

6.1 PIMC Cluster-update Algorithm for Rotational Motion

The most important step of a successful Monte Carlo method is to design a correct and compatible random move for each MC step. Within the GCA algorithm, a 3D unit random vector $\mathbf{v}$ is chosen for molecules in the cluster to reflect. In the rigid rotor approximation model, we treat the rotors as dipoles and rotate those dipoles based on Rodrigues' rotation formula,

$$\mathbf{v}_{\text{rot}} = \mathbf{v}\cos\Delta\theta + (\mathbf{k}\times\mathbf{v})\sin\Delta\theta + \mathbf{k}(\mathbf{k}\cdot\mathbf{v})(1-\cos\Delta\theta) \tag{6.3}$$

where $\mathbf{v}_{rot}$ is the rotated vector, $\mathbf{v}$ is the vector of dipole, and $\mathbf{k}$ is a unit vector describing an axis of rotation about which $\mathbf{v}$ rotates by an angle $\Delta\theta$. A sketch to describe the Rodrigues' formula is shown in Figure 6.1.

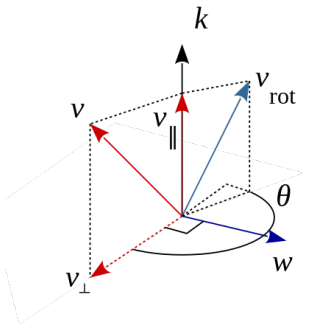

Figure 6.2: Rodrigues-formula

Based on the Rodrigues' formula, we can design a new rotational step for the Monte Carlo method to rotate all particles in the cluster by the same parameters. Moreover, we determine the link between the interior of the cluster and the exterior particles by a link probability, P_{link}.

$$\mathbf{P_{link}} = \max\{1 - \exp[-\tau \Delta V], 0\} \tag{6.4}$$

$$= \max\{1 - \exp[-\tau (V(\mathbf{n}_{i'}, \mathbf{n}_j) - V(\mathbf{n}_{i'}, \mathbf{n}_{j'}))], 0\} \tag{6.5}$$

where $\tau = \beta/P$, and ΔV is the energy difference between the two configurations. $\mathbf{n}_i$ denotes the original vector representation of ith molecule's dipole, and $\mathbf{n}_{i'}$ denotes the rotated vector representation of ith molecule's dipole.

In the presence of an interaction term for beads along the imaginary time path, the cluster-update algorithm should include a cluster acceptance probability given by

$$\mathbf{P_{accept}} = \min\{1, \prod_{c\in\text{cluster}} \frac{\rho^c_{\text{new}}}{\rho^c_{\text{old}}} \times \exp[-\tau\Delta V^{\text{clu}-\text{ext}}]\} \tag{6.6}$$

$$= \min\{1, \prod_{c\in\text{cluster}} \frac{\rho^c_{\text{new}}}{\rho^c_{\text{old}}} \times \exp[-\tau(V^{\text{clu}-\text{ext}}_{\text{new}} - V^{\text{clu}-\text{ext}}_{\text{old}})]\} \tag{6.7}$$

where ρ^c_{old} represents the density matrix element values of the original configuration for cth molecule, ρ^c_{new} represents the density matrix element values of the new configuration for cth molecule, and all $c \in$ cluster in the above equation. $V^{\text{clu}-\text{ext}}_{\text{old}}$ represents the total interacting potential energy between the the cluster molecules and exterior molecules before rotation, and $V^{\text{clu}-\text{ext}}_{\text{new}}$ represents the total interacting potential energy between the the cluster molecules and exterior molecules after rotation. Then, the cluster-update new configurations are only accepted or rejected by this $\mathbf{P_{accept}}$ probability. A outline for the

modified GCA algorithm is shown in Algorithm 6:

Algorithm 6: PIMC Cluster-update Algorithm for Rotational Motion

```
for i < MC step do
    for t in range(P) do
        choose a random molecule a and add a to both cluster clu and buffer buf;
        create a random unit vector k and random angle Δθ;
        rotate a by k and Δθ;
        while buf not empty do
            pop off the first molecule in buf;
            join all nearest neighbor molecules b to the clu an clu by probability
              P_link;
            rotate linked b by k and Δθ;
        end
        for all molecules in clu do
            calculate P_accept;
            if P_accept > 1.0 then
                accept;
            else if P_accept > rand then
                accept
            else
                reject
            end
        end
    end
    calculate the potential and rotational energy;
    calculate the acceptance ratio;
end
```

6.2 System Setup

In order to test this new cluster-update algorithm for a rotational system with on-site interactions, the multi-rotors system of HF molecules with dipole-dipole interaction is chosen. Since we a have well-developed local-update PIMC code in MoRiBS, we will use simulations in MoRiBS as our benchmark calculation. A set of rigid rotors is placed along the z-axis, and simulate the system with different numbers of rotors to test the validity and accuracy of the growth of the cluster for various systems.

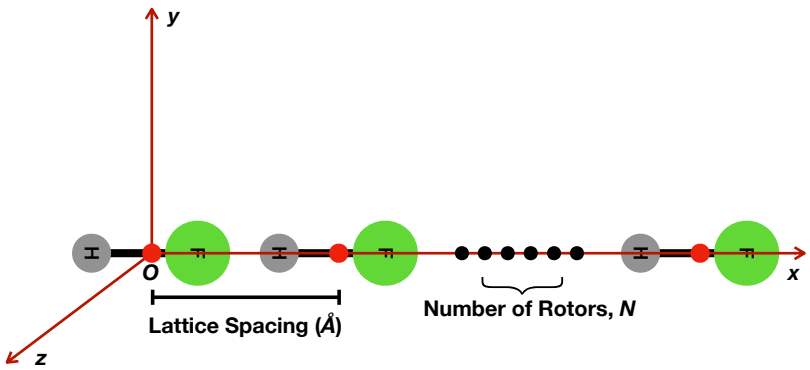

Figure 6.3: PIMC Cluster-update system setup: N HF rotors along x-axis

The parameters used in this set of simulations are presented in Table 6.1. As a very basic test of the validity of the growth of the cluster, we simulate the system at a relatively high temperature, 20.0 K and 16 beads for a various number of rotors.

Table 6.1: The Parameters for the Simulations of N HF Rotors

Parameters	Values
Temperature (T, K)	20.0
Rotational Constant (B, cm^{-1})	20.9557
Number of Rotors (N)	$[2, 3, 4, 5]$
Dipole Moment (d, Debye)	2.0
Simulation Step	500000
Simulation Skip Step	100.0
Number of Beads (P)	[16]
Acceptance Ratio	$(0.3, 0.5)$

6.3 Results

The potential, rotational and total energy τ convergence diagram are shown in Fig. 6.4, Fig. 6.5, and Fig. 6.6 respectively.

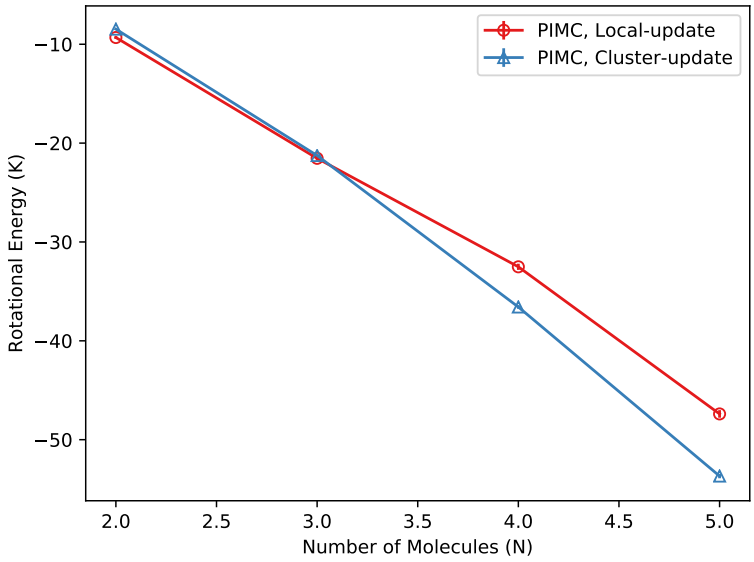

Figure 6.4: Potential energy for HF molecules with different number of molecules at $T = 20.0$ K with $P = 16$. Red points and lines are from local-update PIMC calculation, and blue points and lines are calculated from cluster-update PIMC simulations.

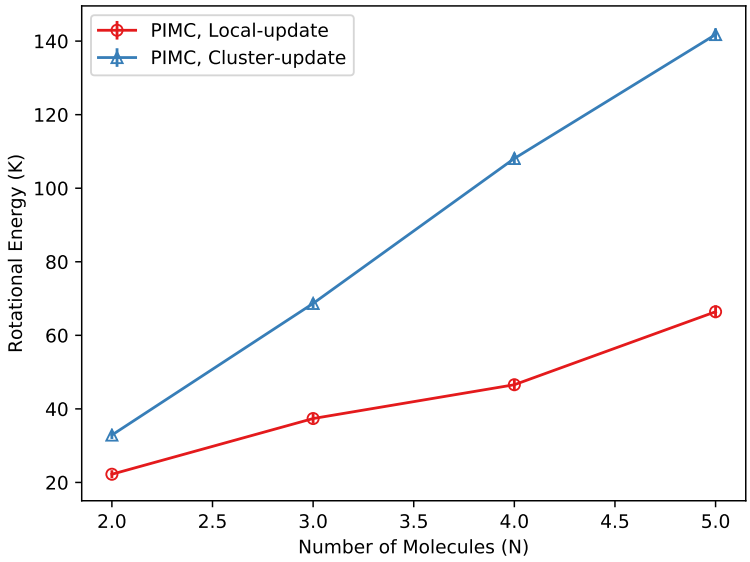

Figure 6.5: Rotational energy for HF molecules with different number of molecules at $T = 20.0$ K with $P = 16$. Red points and lines are from local-update PIMC calculation, and blue points and lines are calculated from cluster-update PIMC simulations.

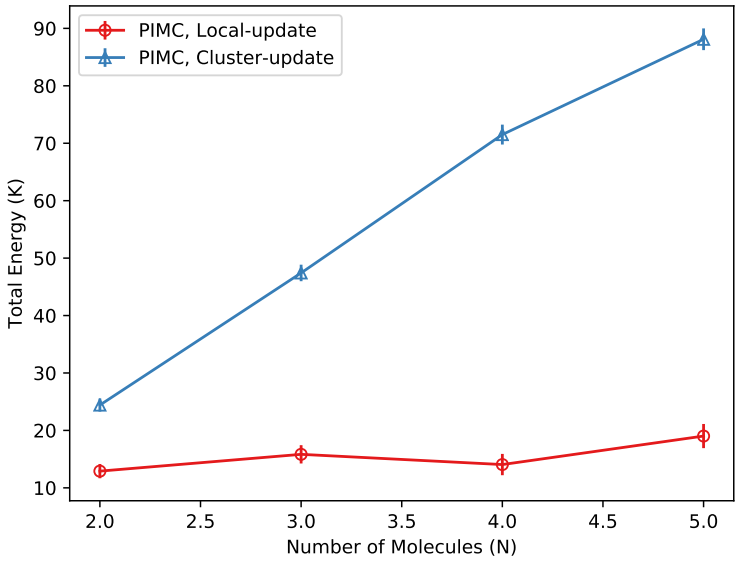

Figure 6.6: Total energy for HF molecules with different number of molecules at $T = 20.0$ K with $P = 16$. Red points and lines are from local-update PIMC calculation, and blue points and lines are calculated from cluster-update PIMC simulations.

For the potential energy calculation in the cluster-update algorithm, a good match can be observed between cluster-update and local-update. However, a large discrepancy also can be found in both rotational and total energy which indicates a problem of our code in essence.

6.4 Discussion

By studying the principle of the cluster-update algorithm, we noticed that a specific Monte Carlo move is required in this new method. When the cluster grows based on the link probability, the whole configuration of the interior of the cluster should be equivalent before and after a random move. Since our force field is anisotropic, the different directions of our dipoles may result in different interior energy. It will cause a failure of the detailed balance requirement for the general Monte Carlo method. For a local-update Monte Carlo method, we have already known, the Monte Carlo random move transforms the configuration a to b has a transition probability $P(a \to b)$. And configurations a and b also have their own probability $\pi(a)$ and $\pi(b)$. Thus, the fundamental condition of detailed balance expressed as

$$\pi(a)P(a \to b) = \pi(b)P(b \to a) \tag{6.8}$$

However, $P(a \to b)$ is not the end of the story, it is a composite probability with two components: considering probability, $\mathcal{A}(a \to b)$, and accepting probability, $\tilde{P}(a \to b)$.

As for Metropolis-Hasting algorithm introduced in Chapter 2, we have the so-called acceptance ratio as

$$\tilde{P}(a \to b) = \min[1, \frac{\pi(b)}{\mathcal{A}(a \to b)} \frac{\mathcal{A}(b \to a)}{\pi(a)}] \tag{6.9}$$

Therefore, a general Monte Carlo method requires three conditions: ergodicity, possibility to compute $\frac{\pi(b)}{\pi(a)}$, possibility to compute $\frac{\mathcal{A}(a \to b)}{\mathcal{A}(b \to a)}$.

As for our case, the cluster-update Monte Carlo algorithm, we need to find the relationship between the cluster link (or growth) probability and the ratio of acceptance ratio. We can consider the following case shown in Fig 6.7,

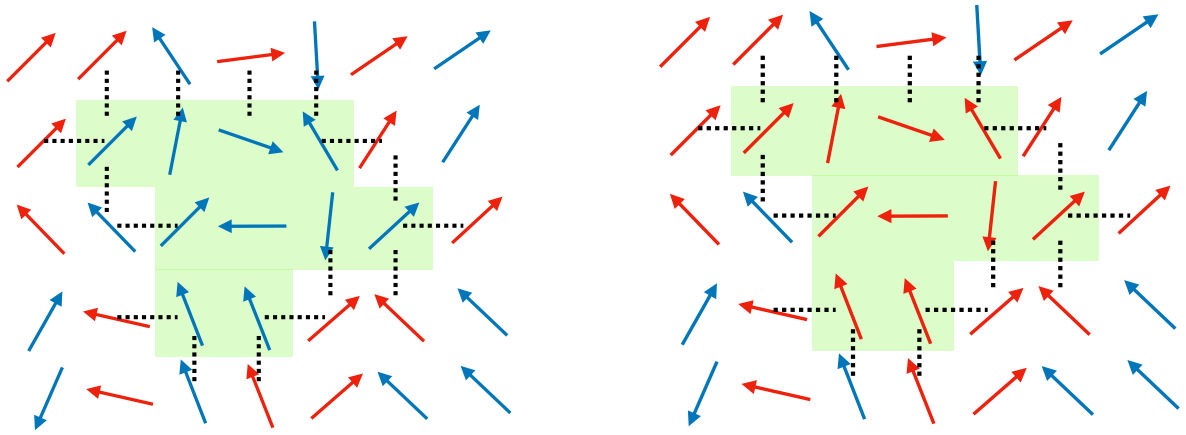

(a) (b)

Figure 6.7: A link can be connected and added to the cluster (green rectangular) by a probability p. (a) configuration a with 10 particles in the cluster with specific construction (blue arrows in green area) (b) configuration b with 10 particles in the cluster with specific construction (red arrows in green area); blue and red arrows represent the dipole vectors of particles, and the same blue or red color means a "linking" preference between these particles, the different color represents a "breaking" preference between particles, black dashed lines represent the links need to be determined between the particles touching the boundary in the cluster and outside of the cluster.

the interior of the clusters (green areas) in the a configuration and the b configuration are distinguished as "same" configurations, but actually, they are the "reflection" configuration to each other. And in a symmetric force field, they can be thought that they have the same relative orientations with respect to the space fixed-frame and they have the same energy inside of the cluster. The real orientations of the particles in the cluster are different between a and b, and also the total energy of the whole configurations are different too.

From the Figure 6.7, it can be seen that the cluster of configuration a is stopped by 11 "blue-red" links, and the cluster of configuration b is stopped by 5 "blue-red" links. Then, we can formulate the considering probability as follows,

$$\mathcal{A}(a \to b) = \mathcal{A}_{\text{interior}} \times (1-p)^{11} \tag{6.10}$$

$$\mathcal{A}(b \to a) = \mathcal{A}_{\text{interior}} \times (1-p)^{5} \tag{6.11}$$

$$E_a = E_{\text{interior}} + E_{\text{exterior}} - g(11) + g(5) \tag{6.12}$$

$$E_b = E_{\text{interior}} + E_{\text{exterior}} - g(5) + g(11) \tag{6.13}$$

where g represents a general function for the energy in terms of the number of particles, and the "interior" means the particles are in the cluster but does not touch the boundary, and the "exterior" means the particles are not in the cluster and also does not touch the

boundary. If we consider a general case, that the stopped link for a is n, and stopped link for b is m, the acceptance ratio now becomes

$$\tilde{P}(a \to b) = \min\left[1, \frac{\exp[-\beta E_b]}{\mathcal{A}_{\text{interior}} \times (1-p)^n} \frac{\mathcal{A}_{\text{interior}} \times (1-p)^m}{\exp[-\beta E_a]}\right] \tag{6.14}$$

$$= \min\left[1, \frac{\exp[-\beta(-g(m)+g(n))]}{(1-p)^n} \frac{(1-p)^m}{\exp[-\beta(-g(n)+g(m))]}\right] \tag{6.15}$$

From the equation above, n and m values are known during the cluster growth. Thus, the link probability p and also the energy difference $g(m) - g(n)$ only depend on the particles of the boundary of the cluster. Also, it will require an "equivalent" configuration of the interior of the cluster to satisfy the detailed balance condition.

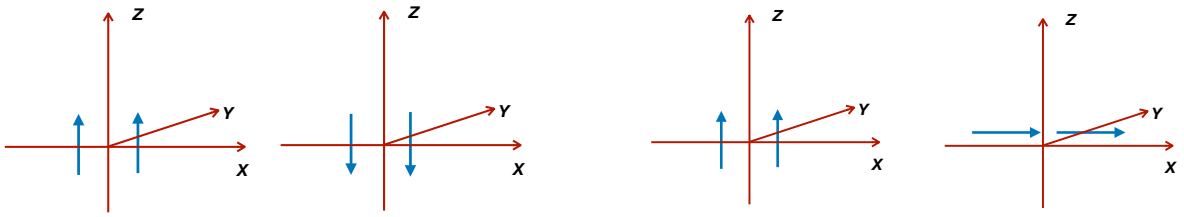

(a) (b)

Figure 6.8: Illustration of two dipoles in a dipole-dipole interaction force field, (a) an equivalent configuration with same relative angles between the two dipoles, (b) an inequivalent configuration still with same relative angles between the two dipoles.

Since the Monte Carlo step is designed based on the relative orientations between the

nearest neighbouring particles which are expressed as the dot product between the nearest neighbouring particles. However, in our case, an anisotropic force field will lead to an antisymmetric configuration. For instance, the dipole-dipole interaction analytical form from Equation (6.2), the z component has a different magnitude compared to the x and y components and causes an antisymmetric force field. Also, from Figure 6.8, it can be observed that even if the two dipoles in two configurations have the same relative angles, the energies are different due to the anisotropic force field. It could arise the "inequivalent configuration" problem which is challenging to develop our cluster-update Path Integral Monte Carlo algorithm.

Chapter 7

Conclusions and Future Work

7.1 Concluding Remarks

Overall, the primary objective of this thesis was to develop a novel methodology to study rotating quantum particles. In Chapter 3, we benchmarked our rotational PIMC code as implemented in MMTK against exact diagonalization calculations and a dCMC code for both linear and asymmetric top molecules. We have confirmed that energetic results agree very well with our benchmark calculations. We however observed issues associated with the non-ergodic behaviour of the local-update PIMC code.

In Chapter 4, we applied our dCMC code to a system consisting of a 1D water chain for a wide range of temperatures and lattice spacings. We were able to predict the behaviour of the water chain system with phase transition plots. Two significant phase transition points and three phase regions were observed vias the use of order parameters. With a lattice spacing between water molecules at around 3.1 Å and 3.9 Å, there are two obvious

transitions indicating different dominant interactions at different lattice spacing. The usual hydrogen-bonding associated with 1D water alignment yields to a 31° angle between the molecular dipoles and the z-axis of the chain. This means that hydrogen bonding interactions yield less alignment along the axis of the chain than pure dipole-dipole alignment. We can deduce that three regimes exist. They are categorized as a "repulsive region" where repulsive interaction is dominant, and hydrogen bonds are broken in this region. The "hydrogen-bonding region" is where the hydrogen bonding interaction dominates. Finally, a "dipole-dipole region" appears when water molecules have a large enough lattice spacing where long-range interactions dominate. In this region, an arrangement where the dipole axis of the water is parallel to the z-axis is favoured due to the dipole-dipole interaction.

In Chapter 5, we tested our hybrid PIMD/PIMC code for the CO_2-He system at 1.0 K for a varying number of beads. We calculated and compared three energy components with MoRiBS pure PIMC simulations, and reached a good agreement. Also, we explored the relationship between rotational skip step N_{rsk} and energy values and found as a preliminary result that the energy fluctuates around the correct pure PIMC results from the MoRiBS calculations. This may indicate a non-converged simulation and the relationship of the time-scale between translation and rotation still remains to be clarified.

Finally, in Chapter 6, we modified one of the cluster-update algorithms, GCA, to develop our own cluster-update MC method for the quantum rotors. We calculated the

potential and rotational energy and observed that only the potential energy agrees well with our reference local update approach for systems consisting of a small number of rotors. However, the rotational and total energy exhibit large discrepancies compared to the local-update results. We have also studied the whole procedure and theory behind the cluster-update Monte Carlo method. The detailed balance condition was evaluated and studied under the cluster-update situation. An equivalent configuration of the cluster interior is required to satisfy the detailed balance condition. In the case of dipole interactions, the anisotropy makes it challenging to design a proper Monte Carlo rotational step that satisfies detailed balance. A new MC random move for rotation should therefore be developed.

7.2 Future Work

There are a number of suggestions for future work based on the developments presented in this thesis. One clear direction for our hybrid PIMD/PIMC code is to perform an energy convergence study, and benchmark against an exact basis set calculations. Also, more parallel calculations are required for us to explore the relationship and time-scale between translational and rotational motions. In addition to these validation tests, we can also enhance our code so that it can simulate a larger system with a better performance via the use of libraries such as the OpenMM accelerated MMTK program implemented by Bishop

et al in 2015 and also the umbrella sampling method in 2018 to study the free energy profiles of quantum systems [63, 64].

Another area of future research would be the design of a new Monte Carlo move for rotational systems to further develop our cluster-update algorithm. Work has been reported in the literature where the Wolff algorithm has been applied to the anisotropic continuous-spin model [65]. The authors propose a solution to the problem of the antisymmetric configurations by decomposing the spins into components parallel and perpendicular to a random unit vector $\mathbf{n}$ which controls the reflection among spins. They treated the component which contributes to the cluster growth in an isotropic case as the main part of the Wolff's algorithm, and the other anisotropic part became a local on-site field acting on every spin. It would be beneficial to determine if these modifications are valid and work for our cluster-update algorithm. Once a solution is found, a novel cluster-update Monte Carlo algorithm can be proposed for rotational systems. This would enhance PIMC sampling and reduce simulation time. Also, since the system is no longer evolved using local updates, decorrelated configurations can be generated more efficiently. Overall, both the simulation and correlation time would be reduced if a cluster algorithm is developed.

References

[1] R. P. Feynman and A. R. Hibbs, *Quantum mechanics and path integration* (1965).

[2] K. Hinsen, Journal of Computational Chemistry, **21, 2**, 79 (2000).

[3] C. Ing, K. Hinsen, J. Yang, T. Zeng, H. Li, and P.-N. Roy, The Journal of Chemical Physics, **136, 22**, 224309 (2012).

[4] M. Schmidt and P.-N. Roy, Journal of Chemical Physics, **148, 12** (2018).

[5] R. H. Swendsen and J.-S. Wang, Physical review letters, **58, 2**, 86 (1987).

[6] U. Wolff, Physical review letters, **62**, 361 (1989).

[7] C. Dress and W. Krauth, Journal of Physics A: Mathematical and General, **28, 23**, L597 (1995).

[8] D. A. McQuarrie, *Quantum Chemistry*, University Science Books, 2 edition (2007).

[9] R. N. Zare, *Angular Momentum: Understanding Spatial Aspects in Chemistry and Physics*, Wiley-Interscience (1991).

[10] R. Feynman and H. Kleinert, Physical review. A, General physics, **34, 6**, 5080 (1986).

[11] D. Marx and M. H. Müser, Journal of Physics: Condensed Matter, **11, 11**, R117 (1999).

[12] N. Blinov, X. Song, and P.-N. Roy, Journal of Chemical Physics, **120, 13**, 5916 (2004).

[13] M. H. Müser, Molecular Simulation, **17, 3**, 131 (2006).

[14] M. Parrinello and A. Rahman, The Journal of chemical physics, **80, 2**, 860 (1984).

[15] M. E. Tuckerman, Quantum Simulations of Complex Many-Body Systems: From Theory to Algorithms, **10**, 269 (2002).

[16] M. Ceriotti, M. Parrinello, T. E. Markland, and D. E. Manolopoulos, The Journal of Chemical Physics, **133, 12**, 124104 (2010).

[17] Trotter, H F, Proceedings of the American Mathematical Society, **10, 4**, 545 (1959).

[18] D. M. Ceperley, Reviews of Modern Physics, **67, 2**, 279 (1995).

[19] M. Suzuki, Physics Letters A, **180, 3**, 232 (1993).

[20] D. Marx, Molecular Simulation, **12, 1**, 33 (1994).

[21] E. G. Noya, C. Vega, and C. McBride, The Journal of Chemical Physics, **134, 5**, 054117 (2011).

[22] M. E. Rose, *Elementary Theory of Angular Momentum*, Courier Corporation (1995).

[23] A. Krachmalnicoff, R. Bounds, S. Mamone, S. Alom, M. Concistrè, B. Meier, K. Kouřil, M. E. Light, M. R. Johnson, S. Rols, A. J. Horsewill, A. Shugai, U. Nagel, T. Rõõm, M. Carravetta, M. H. Levitt, and R. J. Whitby, Nature Chemistry, **8, 10**, 953 (2016).

[24] S. Mamone, M. Ge, D. Hüvonen, U. Nagel, A. Danquigny, F. Cuda, M. C. Grossel, Y. Murata, K. Komatsu, M. H. Levitt, T. Rõõm, and M. Carravetta, Journal of Chemical Physics, **130, 8**, 081103 (2009).

[25] J. Hernández-Rojas, J. Bretón, and J. M. Gomez Llorente, Chemical Physics Letters, **222, 1-2**, 88 (1994).

[26] Y. N. Kalugina and P.-N. Roy, The Journal of Chemical Physics, **147, 24**, 244303 (2017).

[27] T. Halverson, D. Iouchtchenko, and P.-N. Roy, The Journal of Chemical Physics, **148, 7**, 074112 (2018).

[28] M. H. Levitt and A. J. Horsewill, Phil. Trans. R. Soc. A, **371, 1998**, 20130124 (2013).

[29] C. Beduz, M. Carravetta, J. Y. C. Chen, M. Concistrè, M. Denning, M. Frunzi, A. J. Horsewill, O. G. Johannessen, R. Lawler, X. Lei, M. H. Levitt, Y. Li, S. Mamone,

Y. Murata, U. Nagel, T. Nishida, J. Ollivier, S. Rols, T. Rõõm, R. Sarkar, N. J. Turro, and Y. Yang, Proceedings of the National Academy of Sciences, **109, 32**, 12894 (2012).

[30] J. K. Holt, Microfluidics and Nanofluidics, **5, 4**, 425 (2008).

[31] A. Berezhkovskii and G. Hummer, Physical review letters, **89, 6**, 064503 (2002).

[32] M. Thomas, B. Corry, and T. A. Hilder, Small, **10, 8**, 1453 (2014).

[33] M. Majumder, N. Chopra, R. Andrews, and B. J. Hinds, Nature, **438, 7064**, 44 (2005).

[34] J. K. Holt, H. G. Park, Y. Wang, M. Stadermann, A. B. Artyukhin, C. P. Grigoropoulos, A. Noy, and O. Bakajin, Science, **312, 5776**, 1034 (2006).

[35] M. Elimelech and W. A. Phillip, science, **333, 6043**, 712 (2011).

[36] R. Das, M. E. Ali, S. B. A. Hamid, S. Ramakrishna, and Z. Z. Chowdhury, Desalination, **336**, 97 (2014).

[37] S. D. Bernardina, E. Paineau, J.-B. Brubach, P. Judeinstein, S. Rouziere, P. Launois, and P. Roy, Journal of the American Chemical Society, **138, 33**, 10437 (2016).

[38] X. Ma, S. Cambré, W. Wenseleers, S. K. Doorn, and H. Htoon, Physical review letters, **118, 2**, 027402 (2017).

[39] K. V. Agrawal, S. Shimizu, L. W. Drahushuk, D. Kilcoyne, and M. S. Strano, Nature Nanotechnology, **12, 3**, 267 (2017).

[40] P. Kapitza, Nature, **141, 3558**, 74 (1938).

[41] S. Grebenev, J. Toennies, and A. Vilesov, Science (New York, N.Y.), **279, 5359**, 2083 (1998).

[42] H. Li and R. J. Le Roy, Physical chemistry chemical physics : PCCP, **10, 28**, 4128 (2008).

[43] T. Zeng, H. Li, and P.-N. Roy, International Journal of Quantum Chemistry, **115, 9**, 535 (2015).

[44] T. Zeng and P.-N. Roy, Reports on progress in physics. Physical Society (Great Britain), **77, 4**, 046601 (2014).

[45] T. Zeng, N. Blinov, G. Guillon, H. Li, K. P. Bishop, and P.-N. Roy, Computer Physics Communications, **204**, 170 (2016).

[46] N. Hansen and W. F. van Gunsteren, Journal of chemical theory and computation, **10, 7**, 2632 (2014).

[47] M. Herman, E. Bruskin, and B. Berne, The Journal of Chemical Physics, **76, 10**, 5150 (1982).

[48] R. W. Hall and B. J. Berne, The Journal of chemical physics, **81, 8**, 3641 (1984).

[49] E. Luijten, *Introduction to Cluster Monte Carlo Algorithms*, 13–38, Springer Berlin Heidelberg, Berlin, Heidelberg (2006).

[50] L. Hayward Sierens, *Simulating quantum matter through lattice field theories*, UWSpace (2017).

[51] C. McBride, E. G. Noya, and C. Vega, Computer Physics Communications, **184, 3**, 885 (2013).

[52] D. U. Webb and K. N. Rao, Journal of Molecular Spectroscopy, **28, 2**, 121 (1968).

[53] F. Paesani, W. Zhang, D. A. Case, T. E. Cheatham, and G. A. Voth, Journal of Chemical Physics, **125, 18**, 184507 (2006).

[54] S. Habershon, T. E. Markland, and D. E. Manolopoulos, The Journal of Chemical Physics, **131, 2**, 024501 (2009).

[55] W. L. Jorgensen, J. Chandrasekhar, J. D. Madura, R. W. Impey, and M. L. Klein, The Journal of Chemical Physics, **79, 2**, 926 (1998).

[56] V. Babin, G. R. Medders, and F. Paesani, Journal of chemical theory and computation, **10, 4**, 1599 (2014).

[57] V. Babin, C. Leforestier, and F. Paesani, Journal of chemical theory and computation, **9, 12**, 5395 (2013).

[58] G. R. Medders, V. Babin, and F. Paesani, Journal of chemical theory and computation, **10, 8**, 2906 (2014).

[59] R. T. Hall and J. M. Dowling, The Journal of Chemical Physics, **47, 7**, 2454 (1967).

[60] D. Lankhorst, J. Schriever, and J. C. Leyte, Berichte der Bunsengesellschaft für physikalische Chemie, **86, 3**, 215 (2010).

[61] G. Herzberg, *Electronic spectra and electronic structure of polyatomic molecules*, Van Nostrand (1966).

[62] B. Abolins, R. Zillich, and K. Whaley, Journal of Low Temperature Physics, **165, 5-6**, 249 (2011).

[63] K. P. Bishop, S. Constable, N. F. Faruk, and P.-N. Roy, Computer Physics Communications, **191, C**, 203 (2015).

[64] K. P. Bishop and P.-N. Roy, Journal of Chemical Physics, **148, 10** (2018).

[65] M. D'Onorio De Meo and S. K. Oh, Phys. Rev. B, **46**, 257 (1992).

[66] N. Metropolis, A. W. Rosenbluth, M. N. Rosenbluth, A. H. Teller, and E. Teller, The journal of chemical physics, **21, 6**, 1087 (1953).

[67] D. M. Ceperley and B. Bernu, Journal of Chemical Physics, **89, 10**, 6316 (1988).

[68] S. Constable, M. Schmidt, C. Ing, T. Zeng, and P.-N. Roy, The journal of physical chemistry. A, **117, 32**, 7461 (2013).

APPENDICES

Appendix A

Derivations

A.1 Derivation of Diagonalization of Rotation Operator and Electric Field [8]

The Hamiltonian of the rotational molecule in electric field is,

$$\hat{H} = \hat{T}_{\text{rot}} + V_{\text{elec}}(\theta) \tag{A.1}$$

Since the eigenstates of rotation in $|lm\rangle$ basis are already known, the rotational eigenstate should be in the diagonal position of the Hamiltonian matrix:

$$H_{ll} = E_{\text{rot}} = Bl(l+1) \tag{A.2}$$

Then, we calculate the potential energy of electric field on the above system. The analytical equation for the electric field should be,

$$V_{\text{elec}}(\theta) = \vec{d} \cdot \vec{E}_{\text{z}} = |d||E_{\text{z}}| \cos\theta \tag{A.3}$$

Then, we can evaluate the integral in the basis of $|lm\rangle$,

$$\langle l', m'|V_{\text{elec}}(\theta)|l, m\rangle = \langle l', m'||d||E_{\text{z}}| \cos\theta|l, m\rangle \tag{A.4}$$

$$= |d||E_{\text{z}}|\langle l', m'| \cos\theta|l, m\rangle \tag{A.5}$$

$$= |d||E_{\text{z}}| \int_0^{2\pi} \int_0^{\pi} Y_{l'}^{m'}(\theta, \phi)^* \cos\theta Y_l^m(\theta, \phi) \sin\theta d\theta d\phi \tag{A.6}$$

where $Y_l^m(\theta, \phi)$ is sphereical harmonics,

$$Y_l^m(\cos\theta, \phi) = \frac{1}{\sqrt{2\pi}} \tilde{Y}_l^m(\cos\theta) e^{im\phi} \tilde{Y}_l^m(\cos\theta) = (-1)^m \sqrt{\frac{(2l+1)}{2} \cdot \frac{(l-m)!}{(l+m)!}} P_l^m(\cos\theta) \tag{A.7}$$

and the associated Legendre Polynomial function can be expressed in Rodrigues formula $P_l^m(x) = \frac{(1-x^2)^{m/2}}{2^l l!} \frac{d^{l+m}}{dx^{l+m}} (x^2 - 1)^l$.

Finally, we can have the result of the integral, and the elements of the potential operator in the basis set of rotational quantum number can be obtained,

$$\langle l', m'|V_{\text{elec}}|l, m\rangle = |d||E_{\text{z}}| \left(\delta_{m',m}\delta_{l',l+1}\sqrt{\frac{(l-m+1)(l+m+1)}{(2l+1)(2l+3)}} + \delta_{m',m}\delta_{l',l-1}\sqrt{\frac{(l-m)(l+m)}{(2l-1)(2l+1)}} \right) \tag{A.8}$$

A.2 Derivation of the Euler Angles from the Cartesian Coordinates of Asymmetric Top Molecule (Water) [9]

The symmetry group of water molecule is known as C_{2v}, and in body-fixed frame (BFF), the Cartesian coordinates of water molecules are constant but the space-fixed frame (SFF) are different which illustrated in the following sketches.

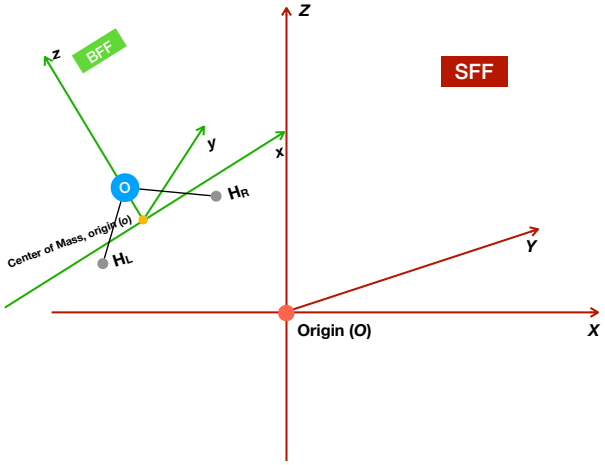

Figure A.1: Illustration of the spaced-fixed frame and body-fixed frame for one water molecule

From the Figure A.1, the water molecule is bound to a body-fixed frame of its own. The convention setup of the coordinates for water molecule in the BFF is fixed, the center of mass of the water molecule is placed at the origin of the BFF. And the oxygen atom is placed at the positive direction of the z-axis, and the first hydrogen atom (referred as H_L) is placed at the negative direction of the x-axis, the second hydrogen atom (referred as H_R) is placed at the positive direction of the x-axis. During rotational and translational motion, the Cartesian coordinates of the water molecule with respect to the SFF are changed, but constant at the BFF. The conventional definition of the Euler angles is also illustrated in Figure A.2,

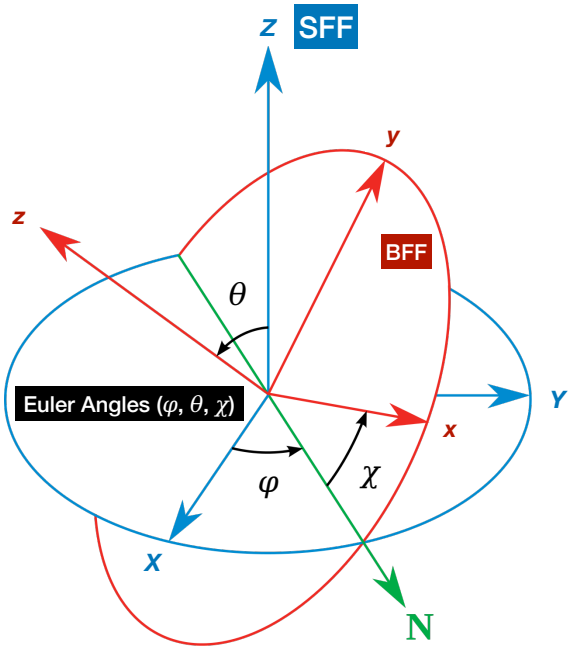

Figure A.2: Illustration of the conventional definition of three Euler angles

Firstly, the whole BFF is rotated about the Z-axis (SFF) by φ so that the x-axis of the BFF is now moved to the new direction and denoted as N-axis and the angle between the N-axis and the X-axis is φ. Then, the BFF is rotated about the N-axis (BFF) by θ, now the z-axis if moved to the new direction, and the new z-axis has an angle θ between the Z-axis (SFF). Finally, the whole BFF is rotated about the new z-axis (BFF) by χ, and the x-axis (BFF) is moved to the new direction and the angle between the N-axis and the new x-axis is χ. Hence, the Euler angles are $\{\varphi, \theta, \chi\}$ and they can determine a 3D-rotation in the space.

After the introduction of the Euler angles definition and the convention water molecule BFF, we now explain how to generate the Euler angles from general Cartesian coordinates of water molecules. Firstly, the Cartesian coordinates of atoms in the water molecule are defined as $\{\mathbf{x}_O, \mathbf{x}_{H_L}, \mathbf{x}_{H_R}\}$.

In order to obtain the Euler angles, the rotational matrix in the principal axes is required to derive from the Cartesian coordinates. Thus, the inertia of tensor, $\mathbf{I}^{\mathbf{SFF}}$for water molecules with respect to the center of mass in the SFF should be calculated at first. In general, the inertia of tensor for a molecule with N atoms can be calculated as follows,

$$\mathbf{I}^{\mathbf{SFF}} = -\sum_{i=1}^{N} m_i[\Delta\mathbf{r}_i]^2 \tag{A.9}$$

where $\Delta\mathbf{r}_i = \mathbf{x}_i - \mathbf{x}_{\mathbf{com}}$ is the relative position vector for atom i which has a mass m_i. It is calculated by the substraction between the Cartesian coordinates of the atom $\mathbf{x}_i$ and the center of mass of the molecule $\mathbf{x}_{\mathbf{com}}$.

Also, it can be evaluated as a matrix form,

$$\mathbf{I}^{\mathbf{SFF}} = \begin{bmatrix} I_{11} & I_{12} & I_{13} \\ I_{21} & I_{22} & I_{23} \\ I_{31} & I_{32} & I_{33} \end{bmatrix} \tag{A.10}$$

the components are defined as

$$I_{jk} = \sum_{i}^{N} m_i(\mathbf{r}^2\delta_{jk} - r_j r_k) \tag{A.11}$$

where $\mathbf{r} = \{r_1, r_2, r_3\}$ still the relative position vector, and it is a 3-dimensional vector which consists of 3 components along different axis $\{r_1, r_2, r_3\} = \{x, y, z\}$.

Then, the principal axes depend on the inertia of tensor with respect to the BFF, not the SFF, which can be evaluated by the diagonalization of the inertia of tensor (SFF), $\mathbf{I^{SFF}}$ because of the following relationship,

$$\mathbf{I^{SFF}} = \mathbf{R}\mathbf{I^{BFF}}\mathbf{R}^T \tag{A.12}$$

The eigenvector of $\mathbf{I^{SFF}}$ is actually the rotational matrix to transform the BFF to the SFF, $\mathbf{R}$. According to the property of the rotational matrix, all rotational matrices are unitary, which means the transpose of $\mathbf{R}$ has the relationship as $\mathbf{R}^T = \mathbf{R}^{-1}$. $\mathbf{R}^{-1}$ is the inverse of $\mathbf{R}$. Also, the diagonalized $\mathbf{I^{SFF}}$ can be denoted as $\mathbf{I^{diag}}$, and has the following form,

$$\mathbf{I}^{\mathbf{diag}} = \begin{bmatrix} I_1 & 0 & 0 \\ 0 & I_2 & 0 \\ 0 & 0 & I_3 \end{bmatrix} \tag{A.13}$$

where and the constants I_1, I_2, and I_3 are named as the principal moments of inertia.

However, the rotational matrix $\mathbf{R}$ and the diagonal inertia of tensor $\mathbf{I}^{\mathbf{diag}}$ right now, are unsorted with respect to the conventional definition of the principal axes for water molecules.

According to the conventional principal axes definition of water molecules, the rows of $\mathbf{I}^{\mathbf{diag}}$ should be sorted by the values of I_1, I_2, and I_3, where the smallest one should be in the first row, and then the second large one, finally the largest value should be in the third row. Then, the corresponding rotational matrix should also be sorted by the corresponding moments of inertia values. Thus, the sorted principal inertia of tensor is now,

$$\mathbf{I}^{\mathbf{diag}} = \begin{bmatrix} I_a & 0 & 0 \\ 0 & I_b & 0 \\ 0 & 0 & I_c \end{bmatrix} \tag{A.14}$$

where $I_a < I_b < I_c$ and similar sorting process for the rotational matrix, $\mathbf{R}$, and generate the sorted one, $\mathbf{R}^{\mathbf{sorted}}$

Furthermore, the convention of the principal axes for water molecules defines I_a axis as the x-axis, I_b axis as the z-axis, and I_c axis as the y-axis. So we need one more step to rearrange the rotational matrix with respect to the BFF axes for water molecules as follows,

$$\mathbf{R}^{\mathbf{principal}} = \mathbf{BFF}^{\mathbf{axis}}\mathbf{R}^{\mathbf{sorted}} \tag{A.15}$$

$$\mathbf{BFF}^{\mathbf{axis}} = \begin{bmatrix} 1 & 0 & 0 \\ 0 & 0 & 1 \\ 0 & 1 & 0 \end{bmatrix} \tag{A.16}$$

Hence, the principal rotational matrix based on the convention principal axes of water molecules is generated. Also, the principal rotational matrix should also be checked if the principal axes after the rotational motion obey the right-hand rule. Then, the Euler angles $\{\varphi, \theta, \chi\}$ can be evaluated from the rotational matrix based on the following formula,

$$\mathbf{R}^{\mathbf{principal}} = \begin{bmatrix} \cos\chi\cos\theta\cos\varphi - \sin\varphi\sin\chi & \cos\chi\cos\theta\sin\varphi + \cos\varphi\sin\chi & -\cos\chi\sin\theta \\ -\sin\chi\cos\theta\cos\varphi - \sin\varphi\sin\chi & -\sin\chi\cos\theta\sin\varphi + \cos\varphi\sin\chi & \sin\chi\sin\theta \\ \sin\theta\cos\varphi & \sin\theta\sin\varphi & \cos\theta \end{bmatrix} \tag{A.17}$$